

1 **Towards an Indian Land Data Assimilation System (ILDAS): A coupled**
2 **hydrologic-hydraulic system for water balance assessments**

3 Bhanu Magotra^a, Ved Prakash^a, Manabendra Saharia^{a,b}, Augusto Getirana^{c,d}, Sujay
4 Kumar^c, Rohit Pradhan^e, C.T. Dhanya^a, Balaji Rajagopalan^f, Raghavendra P. Singh^g,
5 Ayush Pandey^a, Mrutyunjay Mohapatra^h

6 ^aDepartment of Civil Engineering, Indian Institute of Technology Delhi, Hauz Khas,
7 New Delhi 110016, India

8 ^bYardi School of Artificial Intelligence, Indian Institute of Technology Delhi, Hauz
9 Khas, New Delhi 110016, India

10 ^cHydrological Sciences Laboratory, NASA Goddard Space Flight Center, Greenbelt,
11 MD, USA

12 ^dScience Applications International Corporation, Greenbelt, MD, United States

13 ^eIndian Institute of Remote Sensing, Indian Space Research Organization, Dehradun,
14 248001, India

15 ^fDepartment of Civil, Environmental and Architectural Engineering & CIRES,
16 University of Colorado, Boulder CO, USA

17 ^gSpace Applications Centre, Indian Space Research Organization, Ahmedabad 380015,
18 India

19 ^hIndian Meteorological Department, New Delhi 110003, India

20 **Corresponding Author:**

21 Manabendra Saharia

22 Indian Institute of Technology Delhi

23 New Delhi, India 110016

24 Office: +91-011-26591260

25 Email: msaharia@iitd.ac.in

ABSTRACT

26
27 Effective management of water resources requires reliable estimates of land surface states
28 and fluxes, including water balance components. But most land surface models run in
29 uncoupled mode and do not produce river discharge at catchment scales to be useful for water
30 resources management applications. Such integrated systems are also rare over India where
31 hydrometeorological extremes have wreaked havoc on the economy and people. So, an
32 Indian Land Data Assimilation System (ILDAS) with a coupled land surface and a
33 hydrodynamic model has been developed and driven by multiple meteorological forcings
34 (0.1° , daily) to estimate land surface states, channel discharge, and floodplain inundation.
35 ILDAS benefits from an integrated framework as well as the largest suite of observation
36 records collected over India and has been used to produce a reanalysis product for 1981-2021
37 using four forcing datasets, namely, Modern-Era Retrospective Analysis for Research and
38 Applications, Version 2 (MERRA-2), Climate Hazards Group InfraRed Precipitation with
39 Station data (CHIRPS), ECMWF's ERA-5, and Indian Meteorological Department (IMD)
40 gridded precipitation. We assessed the uncertainty and bias in these precipitation datasets and
41 validated all major components of the terrestrial water balance, i.e., surface runoff, soil
42 moisture, terrestrial water storage anomalies, evapotranspiration, and streamflow, against a
43 combination of satellite and in situ observation datasets. Our assessment shows that ILDAS
44 can represent the hydrological processes reasonably well over the Indian landmass with IMD
45 precipitation showing the best relative performance. Evaluation against ESA-CCI soil
46 moisture shows that MERRA-2 based estimates outperform the others, whereas ERA-5
47 performs best in simulating evapotranspiration when evaluated against MODIS ET.
48 Evaluations against observed records show that CHIRPS-based estimates have the highest
49 performance in reconstructing surface runoff and streamflow. Once operational, this system
50 will be useful for supporting transboundary water management decision making in the region.

51 **Keywords:** Indian Land Data Assimilation System (ILDAS), water balance assessments,
52 streamflow, south Asia

53 **1. Introduction**

54 Effective water resources management requires consistent and long-term estimates of
55 the terrestrial water balance, usually derived from computational models driven by accurate
56 meteorological forcings and observational inputs. Land surface models (LSMs) are used to
57 mathematically model the various land surface processes critical in transferring energy fluxes
58 and moisture between the land surface and the atmosphere. The primary purpose of an LSM
59 is to simulate the dynamics of water storage, energy, and water fluxes on the surface and
60 subsurface, by using physically based equations (Kirchner, 2006). While LSMs have been
61 used in multiple studies to simulate water balance at a continental scale across the world and
62 over India, an integrated hydrologic-hydraulic system over the Indian subcontinent has not
63 been developed.

64 The Indian mainland consists of complex terrain with a surface elevation ranging from
65 approximately 10 to 8000 meters above mean sea level while having distinct topography that
66 includes eastern and western coastal regions, northern and northeastern mountain ranges,
67 central flood plains, southern peninsula, and western arid regions. Moreover, the Indian
68 climate is quite diverse, with annual mean temperature and precipitation ranging from
69 approximately 7 to 27 °C and 500 to 4900 mm, respectively. Being primarily an agrarian
70 economy, India relies heavily on the long-term and seasonal availability of freshwater.

71 Additionally, many regions of India are often exposed to natural hazards such as floods and
72 droughts, which are associated with intense precipitation during the southwest monsoon and
73 hot and dry summers, respectively (Saharia et al., 2021; Zhang et al., 2017). Moreover, the
74 warming climate has increased the uncertainty in precipitation, further exaggerating the risks
75 associated with short-term and long-term variations in the natural water balance (Ali and
76 Mishra, 2018). Therefore, accurate estimates of land surface states, streamflow, and flood
77 plain inundation are critical in the decision-making process to ensure national food security,
78 natural hazards mitigation, and water resources planning and management. However, to

79 generate these estimates, two primary challenges need to be addressed: (a) the representation
80 of the spatial variability of various land surface processes and the initial states in LSMs for
81 such a complex landmass is difficult (Zhao & Li, 2015), and (b) the models run in a non-
82 operational setting where the LSMs are generally not coupled with a routing model, and
83 thus, lack the ability to provide near real-time estimates of streamflow at catchment scales.
84 To address this, we set up an Indian Land Data Assimilation System (ILDAS), which is based
85 on a land surface and hydrodynamic model coupled in an offline mode (i.e., no feedback
86 between LSM and hydrodynamic model) and is driven by multiple meteorological forcings to
87 generate spatially consistent and high-resolution estimates of land surface states, water
88 balance, and energy fluxes over the Indian mainland.

89 A Land Data Assimilation System (LDAS) facilitates the assimilation of in situ observations
90 and remotely sensed data to improve the accuracy of LSMs through various data assimilation
91 techniques and the use of observation-based atmospheric forcing data (Kumar et al., 2014).
92 The progress towards the development of various LDAS was led by the North American
93 LDAS (NALDAS; Lohmann et al., 2004) and Global LDAS (GLDAS; Rodell et al., 2004),
94 which were initially developed to provide optimal land surface states and fluxes to
95 atmospheric models to improve weather and climate predictions (Xia et al., 2019). With the
96 increasing availability of remotely sensed data, enhanced in situ observation gauge networks
97 and affordable computational power, many regional LDAS have been developed, such as
98 European LDAS (ELDAS; (Jacobs et al., 2008), South American LDAS (SALDAS; (de
99 Goncalves et al., 2006), South Asia LDAS (Ghatak et al., 2018), and Canadian LDAS
100 (CaLDAS; Carrera et al., 2015). The water and energy fluxes, along with other land surface
101 states generated by regional and global LDAS, have found wide usability in various
102 applications such as flood and drought monitoring, climate prediction models, water resource
103 management, and agricultural crop management (Jin et al., 2018; McNally et al., 2017;
104 Sawada and Koike, 2016; Yucel et al., 2015). The ILDAS is built on NASA's Land

105 Information System Framework (LISF; lis.gsfc.nasa.gov), which is an open-source software
106 that enables a multi-model, multi-data approach to land surface modeling (Kumar et al.,
107 2006). As part of a series of studies that will be carried out towards establishing ILDA, this
108 paper presents the results from the first study in which we used the Noah land surface model
109 with multiparameterization options (Noah-MP; Niu et al., 2011) coupled with the
110 Hydrological Modeling and Analysis Platform (HyMAP; Getirana et al., 2017, 2012) to
111 simulate hydrological processes over the Indian landmass using multiple global
112 meteorological forcing datasets, namely, Modern-Era Retrospective Analysis for Research
113 and Applications, Version 2 (MERRA-2; Gelaro et al., 2017), Climate Hazards Group
114 InfraRed Precipitation with Station data (CHIRPS; Funk et al., 2015), ECMWF's ERA-5
115 (ERA-5; Hersbach et al., 2020), and IMD's gridded precipitation over India. The previous
116 studies over India have mainly used LSMs without a coupled hydrodynamic model and are
117 focused primarily on better representation and understanding of various processes involved in
118 energy and water cycle (Attada et al., 2018; Ghodichore et al., 2022; Maity et al., 2017; Nair
119 & Indu, 2019; Patil et al., 2011). In the study conducted using South Asia LDAS (Ghatak et
120 al., 2018), the authors focus on effects of precipitation uncertainty on various hydrological
121 simulations including streamflow over a similar spatial domain as that of ILDA, but it is
122 limited to a relatively short period of evaluation and fewer observed streamflow locations.
123 Moreover, the study does not include streamflow evaluation over India's geographical
124 domain. In this study, we present a comprehensive evaluation of surface runoff, soil moisture,
125 terrestrial water storage anomalies, evapotranspiration, and streamflow. Besides evaluating
126 major components of the water balance, we also assessed the uncertainty and bias due to
127 spatiotemporal heterogeneity in the forcing precipitation by evaluating against the gauge-
128 based gridded precipitation provided by the Indian Meteorological Department (IMD).
129 Overall, the objectives of this study are to:

- 130 (a) set up ILDAS by coupling a land surface and hydrodynamic model to generate a high-
131 resolution reanalysis dataset over the Indian domain.
- 132 (b) quantify the uncertainty and bias in precipitation provided by the global forcings over the
133 Indian mainland.
- 134 (c) evaluate ILDAS nationwide performance by evaluating simulated water balance
135 variables against in situ and satellite-observed products.

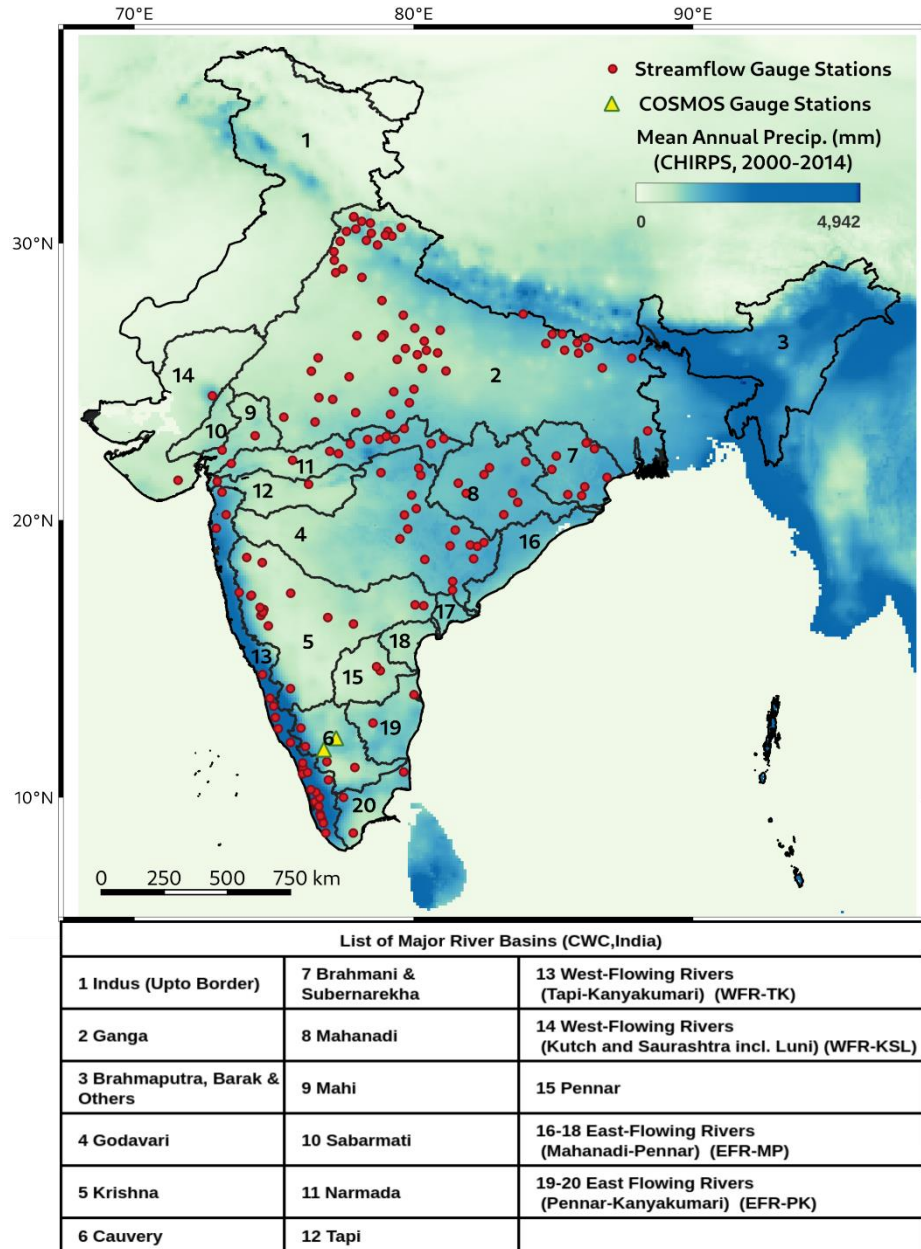
136 The paper is organized as follows: section 2 describes the study area and various datasets
137 used in this study. It also briefly explains the Noah-MP model and the methodology involved
138 in running the model and evaluation of results. In section 3, results are presented along with
139 relevant discussion. Finally, section 4 provides the conclusions of the study and future work.

140 **2. Data and methods**

141 *2.1 Study Area*

142 The modeling system is defined on a spatial domain spanning 68°E – 98°E and 5.5°N
143 – 37.5°N, as shown in (Fig. 1). The landmass primarily consists of the geographical region of
144 India along with some portions of neighboring countries. By taking a wider geographical
145 extent than India's political boundary, we ensured that the LSM could process the necessary
146 meteorological and geological information at the boundary of the Indian landmass. India has
147 a diverse climate and geography that can be attributed to being the world's seventh largest
148 country in terms of area. The Indian mainland includes mountain ranges in the north and
149 north-east, the western and eastern coastal regions, the Indo-Gangetic plains, the desert in
150 western Rajasthan, the peninsular plateau and the islands of Lakshadweep and Andaman and
151 Nicobar. The overall climate of India is considered tropical, with a mixture of dry and wet
152 tropical weather in the country's interior regions. The country gets most of its precipitation
153 from monsoon rains that begin in June and last till September. Although the analysis has been
154 done on a 0.1° spatial resolution grid across the Indian landmass, an attempt has been made

155 to highlight the outcomes based on major river basins as specified by the Central Water
 156 Commission (CWC), India, which are available through the India Water Resources
 157 Information System (IWRIS; www.india-wris.nrsc.gov.in).



158

159 *Fig. 1. A map depicting the ILDAS spatial domain, Indian Central Water Commission*
 160 *River basins and streamflow gauge stations considered in the study.*

161 **2.2 Modeling framework**

162 LISF is an infrastructure that supports multiple land surface models, meteorological
163 forcings, and various data assimilation and routing schemes. Given the scalability and
164 flexibility of LISF, it is well suited for large-scale terrestrial modeling as it enables users to
165 harness high-performance computing and combine various modeling tools and data sources
166 in a systematic and streamlined manner. The Noah land surface model with
167 multiparameterization options (Noah-MP; (G. Y. Niu et al., 2011) builds upon the earlier
168 Noah model (Ek et al., 2003) by including newer land surface physics such as (a) tiling
169 scheme in the grid, which can differentiate between vegetation and bare soil, (b) a multi-layer
170 snowpack as compared to one bulk-layer snowpack, (c) a canopy layer, (d) separation of
171 permeable and non-permeable frozen soil fractions, and (e) TOPMODEL-based runoff
172 scheme along with Simple Groundwater Model (SIMGM; Niu et al., 2007). The Noah-MP
173 also includes multiparameterization options for various physical processes such as runoff
174 generation, dynamic vegetation, canopy stomatal resistance, groundwater, and so on.

175 To simulate discharge and floodplain inundation, we use the coupled Noah-MP with the
176 Hydrological Modeling and Analysis Platform (HyMAP; (A. Getirana, Peters-Lidard, et al.,
177 2017; A. C. V. Getirana et al., 2012) river routing model. HyMAP is a state-of-art global
178 scale hydrodynamic model that uses local inertia formulation to simulate surface water
179 dynamics in rivers and floodplains based on baseflow and surface runoff provided by the
180 LSM at each modeling timestep (Bates et al., 2010; De Almeida et al., 2012). The model
181 employs the local inertia formulation, which involves solving the complete momentum
182 equation of open channel flow. This enables a more stable and efficient representation of
183 river flow diffusiveness and inertia of large water masses with deep flow. Such a
184 representation is important for a physically accurate representation of wetlands, lakes,
185 floodplains, tidal effects, and impoundments (A. Getirana et al., 2020). It adopts a sub-grid
186 approach where both base flow and surface runoff at each grid cell are passed through
187 individual linear reservoirs and adjusted against relevant time delay factors. To derive water

188 storage, elevation and discharge in stream and floodplains, HyMAP processes the
189 topographic information in the form of Digital Elevation Model (DEM), river geometry, and
190 roughness. The HyMAP parameters are derived from the Multi-Error-Removed Improved-
191 Terrain (MERIT; Yamazaki et al., 2017) DEM while the widths of major rivers are derived
192 from MERIT-Hydro which is a 90-m global estimated river width dataset based on Landsat
193 data. However, the width of smaller channels that were not detected by the dataset, was
194 derived using an empirical equation (A. C. V. Getirana et al., 2012):

$$195 \quad w = \max(0.2, 20 \times Q_{med}^{0.5}) \quad (1)$$

196 where w (m) is the average river width within a grid cell and Q_{med} (m^3/s) is the annual mean
197 discharge.

198 River width and bankfull height, h (m) was estimated using the following empirical equation:

$$199 \quad h = \max(0.35, \alpha \times w); \text{ where } \alpha = 2.6 \times 10^{-3} \quad (2)$$

200 The roughness of open channels as well as floodplains is considered in the form of
201 Manning's coefficient, which is based on vegetation type in the individual grid cell (A. C. V.
202 Getirana et al., 2012).

203 ***Model Configuration:***

204 The specifications of various ILNAS parameters are shown in Table 1. The Land Data
205 Toolkit (LDT; Arsenault et al., 2018) was used to generate parameter files that contain
206 various static information to be processed by Noah-MP, such as land use/land cover,
207 irrigation, soil types, elevation, and so on. Four open-loop individual runs were conducted in
208 retrospective mode within the LIS Framework (LISF) on a 0.1x0.1 grid at a 15 minutes
209 timestep. The four runs were conducted from 1981-2021 using MERRA-2, CHIRPS, ERA-5,
210 and IMD, respectively, and the model outputs were produced at daily timestep. In our initial
211 testing, we found that the model reached an equilibrium state over the ILNAS domain after

212 approximately ten years of simulation. We evaluated the equilibrium of the model based on
 213 the percentage difference between the water balance components generated over two
 214 consecutive spin-up runs (Rodell et al., 2005). To ensure that the model has significant
 215 atmospheric information to reach a steady state, we performed two spin-ups for each run with
 216 five years of meteorological data. The simulations were performed in a high-performance
 217 computing facility using 64-100 total CPUs with an average completion time of
 218 approximately 3 hours per year of simulation.

219 Table 1. List of ILDAS components and their specifications.

ILDAS Component	Specifications
Land Surface Model	Noah-MP 3.6
Routing Scheme	HyMAP
Spatial Extent	68°-98°E, 5.5°-37.5°N
Spatial Resolution	0.1°
Temporal Resolution	15 minutes Noah-MP 3.6 and HyMAP with adaptive timestep, daily output fields
Time Period	1981-2021
Forcing	MERRA-2, CHIRPS (precipitation) + MERRA-2, ERA-5, IMD
Forcing Variables	Precipitation, near-surface air temperature, near-surface specific humidity, surface pressure, eastward and northward wind velocity, incident longwave and shortwave radiation
Forcing Height	2 m for surface air temperature, specific humidity, and surface pressure, 10 m for wind
Topography and river network	MERIT Hydro
Soils Definition	(NCAR) STATSGO+FAO blended soil texture map
Vegetation Definition	MODIS-IGBP (NCEP-modified), Monfreda et al. (2008) crop types
Output Format	NetCDF

220 **2.3 Atmospheric Forcings**

221 **2.3.1 MERRA-2**

222 The Modern-Era Retrospective Analysis for Research and Applications, Version 2
223 (MERRA-2; Gelaro et al., 2017) improves upon its predecessor, MERRA, by leveraging
224 recent developments at NASA's Global Modeling and Assimilation Office (GMAO), which
225 include updates to the Goddard Earth Observing System (GEOS) as well as new assimilation
226 schemes for microwave observations, NASA ozone observations, hyperspectral radiance and
227 many more datatypes (Gelaro et al., 2017). In previous studies (Ghatak et al., 2017, 2018;
228 Gupta et al., 2020), MERRA-2 has shown satisfactory results for temperature and
229 precipitation estimates over India. In this study, we used bias-corrected precipitation from the
230 MERRA-2 dataset at a spatial resolution of $0.625^{\circ} \times 0.5^{\circ}$ and hourly timesteps for the period
231 1981-2021.

232 **2.3.2 CHIRPS**

233 Climate Hazards Group InfraRed Precipitation with Station data (CHIRPS; Funk et
234 al., 2015) is a quasi- global precipitation dataset derived from global Cold Cloud Duration
235 (CCD) rainfall estimates calibrated using Tropical Rainfall Measuring Mission Multi-
236 Satellite Precipitation Analysis version 7 (TMPA 3B42 v7). CHIRPS aims to bridge the gap
237 between high latency precipitation products such as Global Precipitation Climatology Centre
238 (GPCC) and low latency satellite-only products like the TMPA 3B42 RT (Funk et al., 2015).
239 The CHIRPS precipitation estimates incorporate in situ gauge station data and active radar
240 satellite systems, and the dataset is available from 1981 to the near present at a high spatial
241 resolution of 0.05° . Since CHIRPS consists of only precipitation, we used MERRA-2 as an
242 overlay to provide other variables in the simulation.

243 **2.3.3 ERA-5**

244 ECMWF's ERA-5 (ERA-5; Hersbach et al., 2020) is a new global reanalysis dataset
245 that builds upon the earlier ERA-Interim reanalysis. The dataset is available from 1959 to
246 present at a spatial resolution of 0.25° and hourly timestep. ERA-5 uses a 10-member
247 ensemble with 12hr 4D-Var data assimilation method to include various reprocessed datasets.
248 The dataset is available in preliminary form at 5 days latency to real time and the final quality
249 assured product is released with a latency of 2 months.

250 **2.3.4 Indian Meteorological Department (IMD) Precipitation**

251 We used gridded daily rainfall data related to the 1981-2021 period at 0.25° spatial
252 resolution provided by the Indian Meteorological Department (IMD). This data is generated
253 using 6955 gauge stations which include IMD observatory stations, hydrometeorological
254 observatories, and Agromet observatories (Pai et al., 2014). To generate gridded data from
255 point-based station rainfall data, an inverse distance weighted interpolation scheme with
256 localized directional effects and barriers was used which is based on (Shepard, 1968). While
257 comparing the observed and reanalysis precipitation products, we rescaled all the datasets to a
258 0.1° spatial resolution. Since IMD precipitation only covers the geographical boundaries of
259 India, we supplemented it with MERRA-2 to provide the missing values beyond IMD
260 precipitation's domain.

261 **2.4. Observed and Satellite Products**

262 The following section covers the suite of satellite-based and in-situ observations that were
263 acquired from various sources for the evaluation.

264 **2.4.1 GRUN (RUNOFF)**

265 We used the GRUN runoff dataset (Ghiggi et al., 2019) as observed data, which is an
266 observationally driven globally reconstructed monthly runoff at 0.5° resolution for the period
267 of 1902-2014. Machine learning-based Random Forest (RF) was used to generate the GRUN
268 runoff data, and the temperature and precipitation gridded data was used from the Global Soil

269 Wetness Project Phase 3 (GSWP3) (Kim & Office, 2017). The Global Streamflow Indices
270 and Metadata archive (GSIM) was used to obtain monthly runoff observations. To test the
271 sensitivity of the machine learning algorithm, Ghiggi et al., (2019) used 50 ensembles. In this
272 study, we used the GRUN reconstruction, which is an ensemble mean of the realizations.

273 **2.4.2 Observed Soil Moisture (COSMOS)**

274 We acquired in-situ observed soil moisture at two-gauge stations (Singanallur-SGR
275 and Adahalli-MDH) from Indian Cosmic Ray Network (ICON; Upadhyaya et al., 2021).
276 ICON consists of seven sites equipped with COSMOS instruments across India operational
277 from 05/2015. The Cosmic Ray Neutron Probe (CRNP) technique is used in the COSMOS
278 instrument, which uses non-invasive neutron counts as a measure of soil moisture. More
279 information can get from webpage <https://cosmos-india.org/>.

280 **2.4.3 ESA-CCI (SATELLITE SOIL MOISTURE)**

281 European space agency's climate change initiative for soil moisture (ESA-CCI SM
282 version v07.1) is used as the soil moisture reference dataset in our study, which is available at
283 0.25° resolution from 1978 (Dorigo et al., 2017; Gruber et al., 2017, 2019). The ESA CCI
284 provides three products, namely Active, Passive, and Combined. While Active products were
285 retrieved from active microwave sensors using the TU Wien water Retrieval Package
286 (WARP) algorithm, their Passive counterparts were obtained using the Land Parameter
287 Retrieval Model (LPRM) algorithm (Owe et al., 2008) from passive-microwave-based
288 sensors. In this study, we used a combined product of the ESA-CCI SM products, which is
289 generated by merging the active and passive products following a decision tree method and
290 has been found to be most suitable for evaluation in the Indian mainland (Chakravorty et al.,
291 2016; Maina et al., 2022).

292 **2.4.4 MODIS Evapotranspiration**

293 We acquired Evapotranspiration from Moderate Resolution Imaging
294 Spectroradiometer (MODIS). We used the MYD16A2GF product (Running et al., 2019), a
295 gap filled at 8-day temporal resolution and 500m spatial resolution. Calculation of ET is
296 typically based on the conservation of either energy or mass or both. The Penman-Monteith
297 equation (J. L. Monteith, 1965) has been used in the ET algorithm.

298 **2.4.5 GRACE TERRESTRIAL WATER STORAGE ANOMALIES (TWSA)**

299 We acquired Gravity Recovery Climate Experiment (GRACE; Landerer and
300 Swenson, 2012; Tellus, 2018) terrestrial water storage anomalies (TWSA) data from the Jet
301 Propulsion Laboratory (JPL). The TWS is obtained using the Mass Concentration blocks
302 (mascons) techniques, which implement geophysical constraints referred to as mascons. Our
303 study used the latest JPL mascon solution (Tellus, 2018; Watkins et al., 2015), which is
304 available monthly at 0.5° spatial resolution. The anomalies are calculated relative to the
305 January 2004-December 2009 as the time-mean baseline and provided as TWSA.

306 **2.4.6 Observed streamflow**

307 The daily streamflow observed records were collected from various government
308 agencies through the public domain as well as official requests. The records were checked for
309 data inconsistencies and were converted to a standard format for analysis. Due to varying
310 record lengths across the gauge stations, a common testing period with enough stations could
311 not be established. We selected gauge stations with at least twenty years of daily recorded
312 values in the period 1981-2021, which may or may not be continuous. In this way, a total of
313 162 stream flow gauge stations were chosen across the study area, as highlighted in (Fig. 1).

314 **2.5 Mann-Kendall Trend Analysis**

315 We used the Mann-Kendall (Mann, 1945) test for trend analysis, which is a non-
316 parametric test for the monotonic trends of environmental data over time, such as climate

317 data or hydrological data (Hu et al., 2020). It is a rank-based significance test, that identifies
 318 the significance of the trend by checking S-statistics of the time series fall in the confidence
 319 interval null hypothesis or not. The S-statistics are calculated to determine whether the trend
 320 is increasing or decreasing.

$$321 \quad S = \sum_{k=1}^{n-1} \sum_{j=k+1}^n \text{sign}(x_j - x_k) \quad (3)$$

322 where x is the time series variable, and the subscripts j and k are the observation time.
 323 $\text{sign}(x_j - x_k)$ is equal to +1, 0, or -1, which means increasing, no, and decreasing trends,
 324 respectively. We rescaled the S-statistics between (-1,1) for better understanding. Here we
 325 assume that there is no significant trend in data at a level of 5% (or 95% confidence interval)
 326 as a null hypothesis.

327 **2.6 Evaluation criteria**

328 To check the effectiveness of different meteorological forcing, we used correlation
 329 coefficient, Relative Root Mean Square Error (RRMSE), and percent bias to evaluate the
 330 annual mean precipitation of reanalyzed meteorological forcings with gridded precipitation
 331 data from IMD.

$$332 \quad RRMSE = \frac{\sqrt{\frac{\sum (p_o - p_r)^2}{N}}}{\frac{\sum p_o}{N}} \quad (4)$$

$$333 \quad Pbias = \frac{\sum (p_r - p_o)}{\sum p_o} \times 100 \% \quad (5)$$

334 where p_o , p_r , and N are Observed, reanalyzed and number of data, respectively.

335 To perform a balanced assessment of simulated water balance against observed values, we
 336 rescaled all the observed datasets to the same resolution of ILDAS for the evaluation of the

337 ILDAS. We selected Kling Gupta Efficiency (KGE; Gupta et al., 2009) as our primary metric
338 with its three components, namely, correlation coefficient (r), variability ratio(α) and bias(β).
339 The calculation of KGE is expressed as:

$$340 \quad KGE = 1 - \sqrt{S_r[r - 1]^2 + S_\alpha[\alpha - 1]^2 + S_\beta[\beta - 1]^2} \quad (6)$$

$$341 \quad \left(\alpha = \frac{\sigma_s}{\sigma_o}, \beta = \frac{\mu_s}{\mu_o} \right)$$

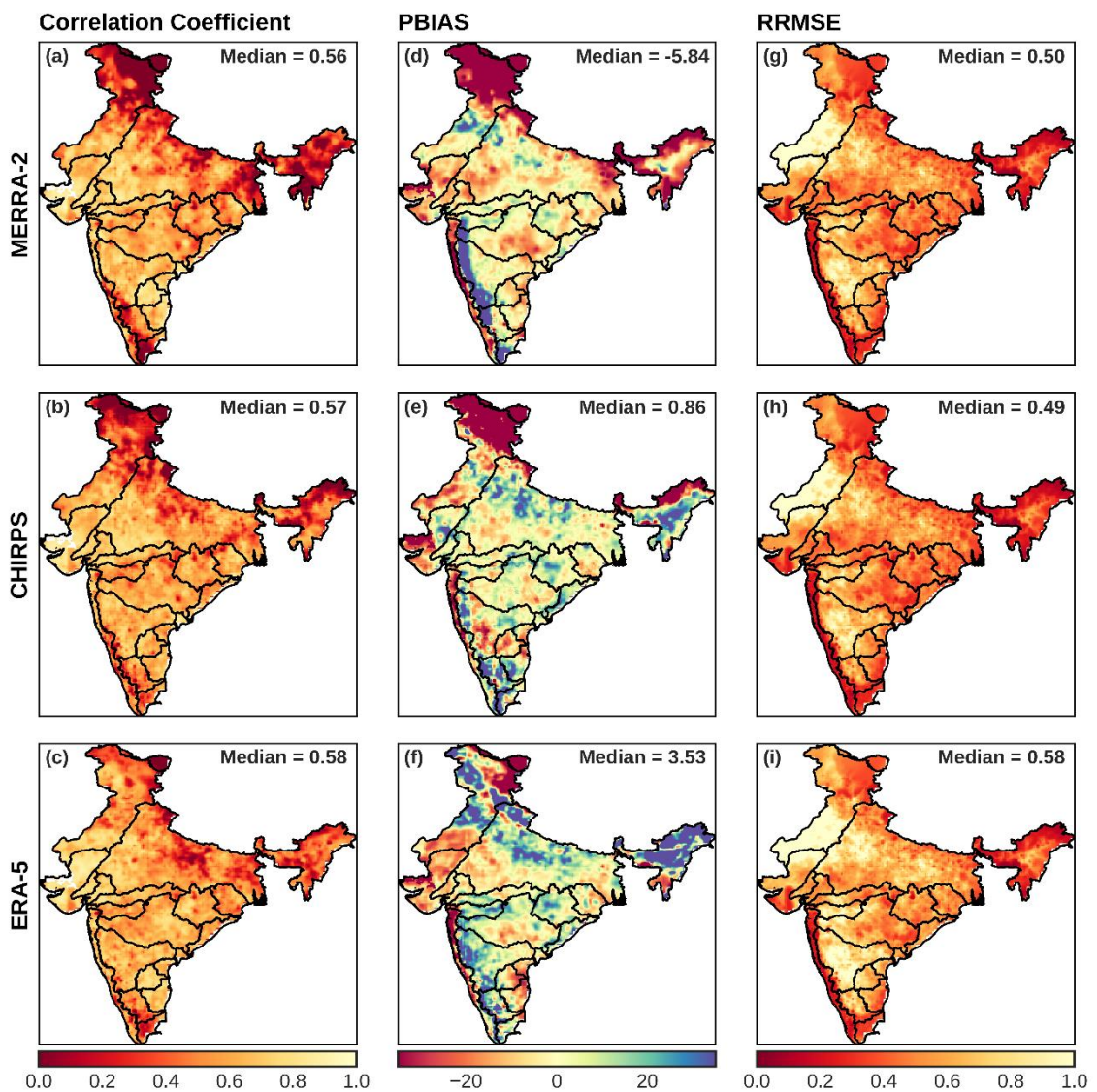
342 where S_r , S_α , and S_β are scaling factors for the three components respectively, that can be
343 specified by the user; σ_s and σ_o are the standard deviations for simulated and observed
344 variables, respectively, and μ_s and μ_o are the corresponding mean values. The three
345 components of KGE highlight different parts of the performance of a model where the
346 agreement between the timing of simulated and observed values is given by correlation (r),
347 the statistical variability is expressed by variability ratio (α), and the bias is highlighted by
348 bias (β). A KGE value equal to 1 ($r=1$, $\alpha=1$, $\beta=1$) means a perfect agreement between
349 simulated and observed values, while a value less than -0.41 denotes that the model is a
350 worse predictor than the mean of the observed series (Knoben et al., 2019). The scaling
351 factors can be used to emphasize one or more components of KGE depending on the
352 objective of the study (Mizukami et al., 2019). In this study, we wanted to present a balanced
353 overview of performance, and therefore, we considered all three scaling factors equal to 1.0.
354 Moreover, considering the wide differences in soil moisture obtained from models, satellites,
355 and in-situ observations, we used anomaly correlation and unbiased RMSE (ubRMSE)
356 instead of KGE for an objective evaluation of the variable.

357 **3. Results and discussion**

358 ***3.1 Precipitation analysis***

359 A significant uncertainty in hydrological models comes from meteorological forcings,
360 particularly precipitation. In particular, the precipitation frequency distribution is the most
361 important factor for the accurate characterization of frequent and extreme floods (Newman et
362 al., 2021). To check consistency, we evaluated the meteorological forcing inputs from 1981
363 to 2021 against the IMD gridded observed precipitation dataset. Overall, ERA-5 shows a
364 better national median correlation (median value of the correlation for all gridded values in
365 the Indian mainland) compared to MERRA-2 and CHIRPS. It also shows a better correlation
366 with IMD in the Himalayan and northeast regions than MERRA-2 and CHIRPS (Fig. 2a-c).
367 However, MERRA-2 shows a better correlation in Rajasthan and Deccan plateau than
368 CHIRPS and ERA-5 meteorological forcing precipitation. In all three meteorological
369 forcings, we found that precipitation is underestimated (i.e., percent bias shows negative
370 values) in the Western Ghats, Himalayan, and northeastern region (Fig. 2d-f). General
371 underestimation in satellite precipitation over the Himalayan region has also been reported by
372 Bharti and Singh, (2015) due to satellites missing the convective clouds. CHIRPS indicates
373 positive Pbias (overestimation) in parts of northeast India. In the northern plane and Deccan
374 plateau, CHIRPS and ERA-5 show overestimation (positive Pbias) compared to MERRA-2.
375 Moreover, CHIRPS and ERA-5 show a nationwide median of Pbias positive
376 (overestimation), whereas MERRA-2 shows underestimation. Underestimation in the
377 Western Ghats might be due to the radiometrically warm land surface, and the coastal regions
378 are a mixture of the radiometrically cold oceans (Mccollum & Ferraro, 2005; Shah & Mishra,
379 2016). We also found that RRMSE is higher in the Western Ghats, Himalayan, and northeast
380 regions than in the Deccan plateau and Rajasthan (semiarid areas) (Fig. 2g-i). Moreover, all
381 metrological forcings show improvement in RRMSE for the monsoon (JJAS) period (Fig.
382 S4). Fig. 3a shows the annual mean precipitation for IMD, MERRA-2, CHIRPS, and ERA-5.
383 We identified that MERRA2 underestimates the annual mean precipitation compared to other
384 forcings till 2009, which is consistent with the observations of a previous study

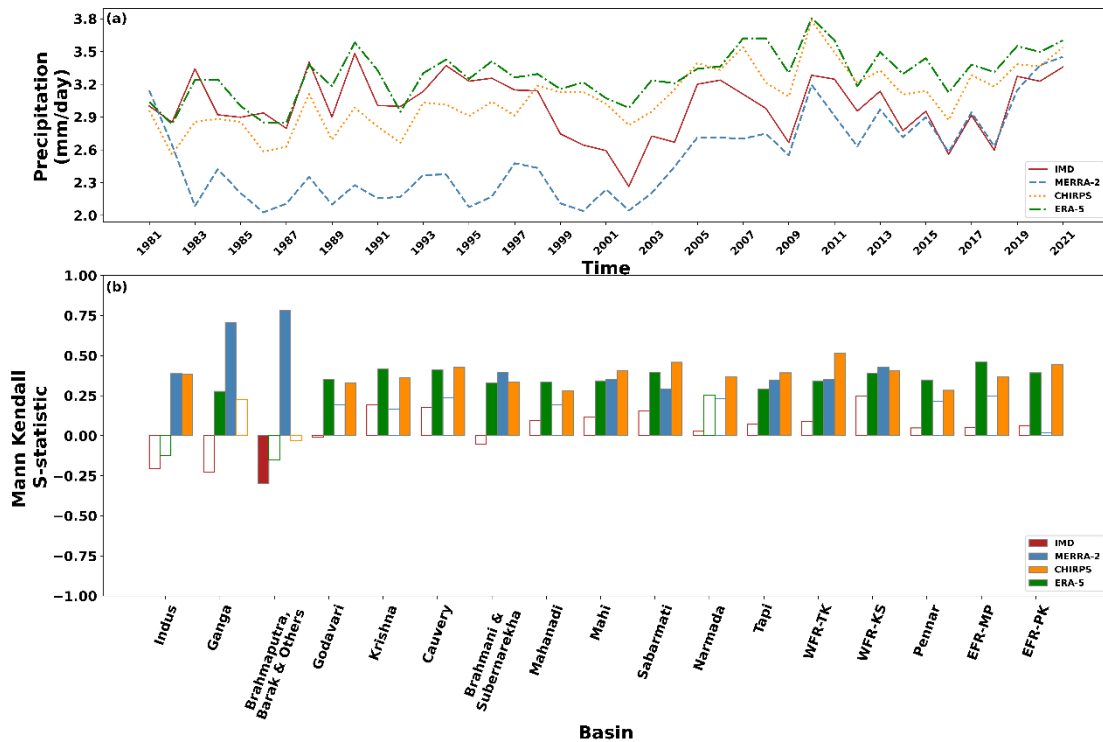
385 (Bhattacharyya et al., 2022). From the figure, it is clear that all meteorological forcings are
 386 showing a significant positive trend ($p < 0.05$) unlike IMD for most of the basins. MERRA-2
 387 displayed an increasing trend in the Himalayan regions, a pattern similar to what was found
 388 by Yoon et al., (2019). Overall, our analysis shows that CHIRPS is less uncertain than
 389 MERRA-2 and ERA-5 with IMD as the baseline.
 390



391

392 *Fig. 2. Comparison of correlation coefficient (a-c), Pbias (d-f), and RRMSE (g-i) of*
 393 *Annual precipitation for different precipitation datasets (i.e., MERRA-2, CHIRPS, and ERA-*

394 5) with respect to the India Meteorological Department (IMD) precipitation dataset for 1981-
395 2021.



396
397 Fig. 3. Nationwide mean annual precipitation plot for different precipitation datasets (IMD,
398 MERRA-2, CHIRPS, ERA-5) for 1981-2021(a) and basin wise precipitation Mann Kendall
399 (M.K.) trend analysis, colored boxes show a significant trend (b).

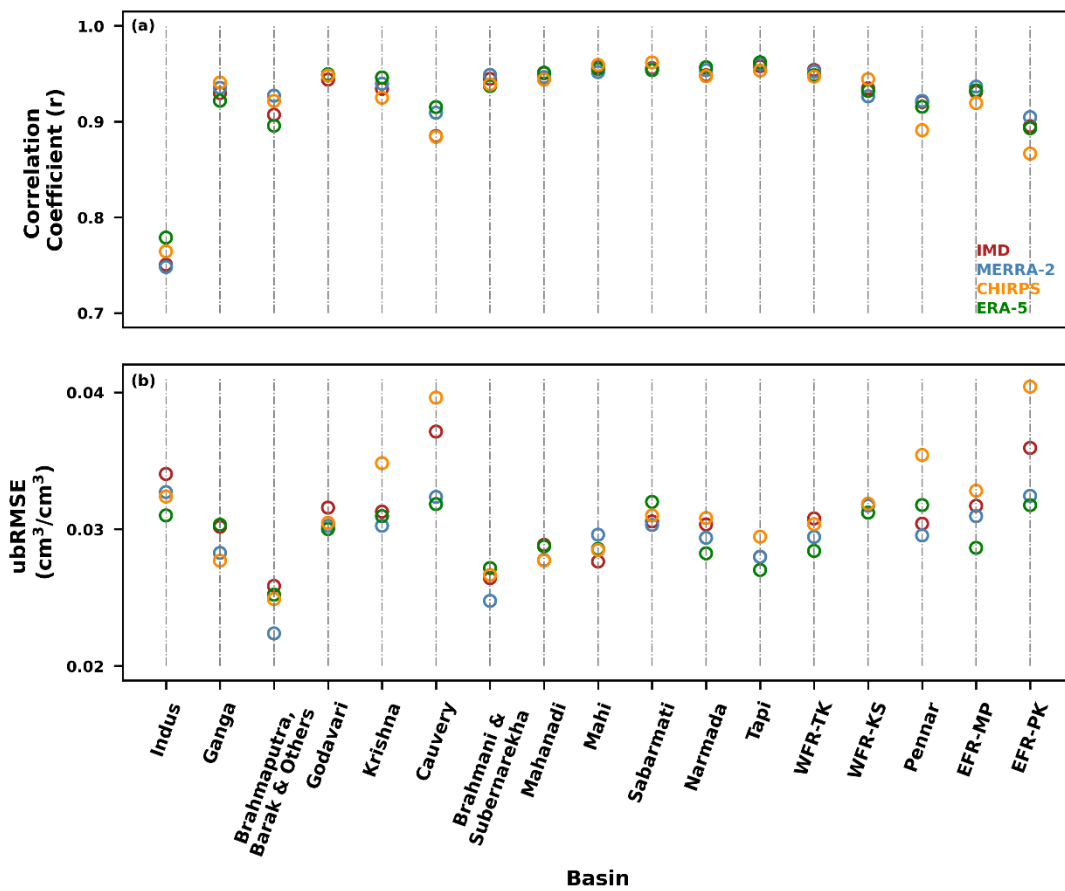
400 3.2. Model output evaluation

401 3.2.1. Soil moisture

402 To evaluate the ability of the ILDAS to simulate soil moisture, we calculated the
403 coefficient of correlation and unbiased RMSE (Fig. 4) of simulated monthly mean soil
404 moisture anomalies with ESA-CCI monthly mean soil moisture anomalies for the period of
405 2007 to 2021. The period is selected based on continuous data availability without gaps over
406 India. After evaluating the basin-wise coefficient of correlation median values over the
407 primary basins, we found that MERRA-2 shows a high correlation in most of the basins, with

408 the highest in the west flowing rivers from Tapi to Kanyakumari (0.95) (Fig. 4a). Kantha Rao
 409 and Rakesh, (2019) also found a high correlation of simulated soil moisture and in-situ
 410 observations in the coastal regions. We found that MERRA-2 and ERA-5 show less ubRMSE
 411 compared to CHIRPS and IMD in most of the basins (Fig. 4b).

412

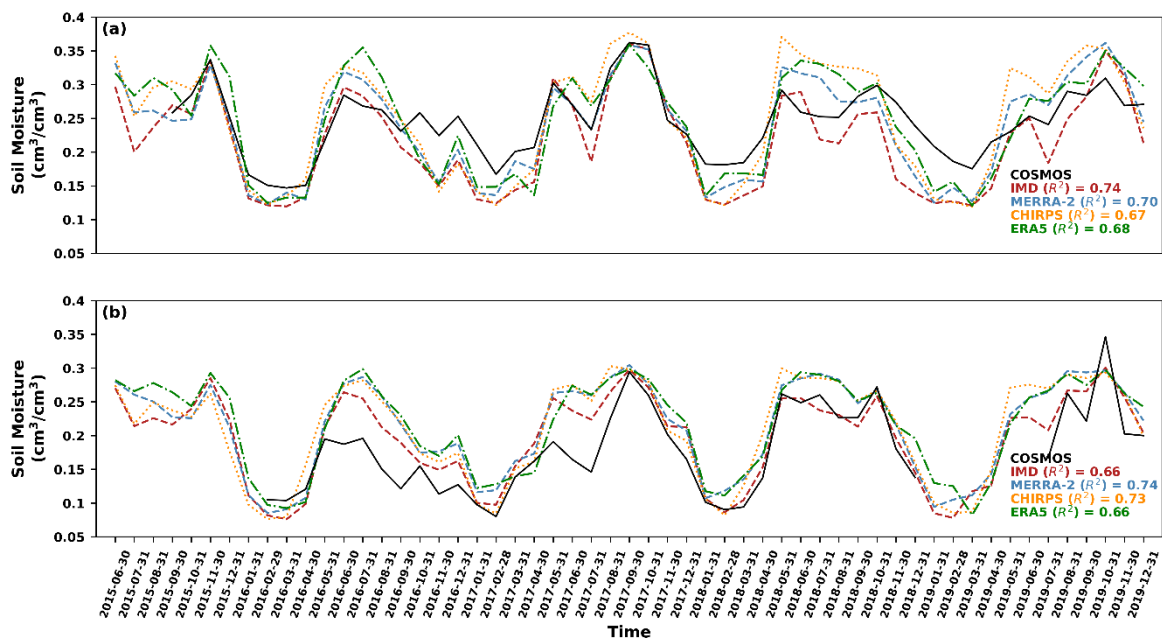


413

414 *Fig. 4. Basin-wise comparison of correlation, and unbiased RMSE of simulated*
 415 *monthly soil moisture anomalies for different meteorological forcings (IMD, MERRA-2,*
 416 *CHIRPS, and ERA-5) with ESA-CCI soil moisture anomalies for 2007-2021.*

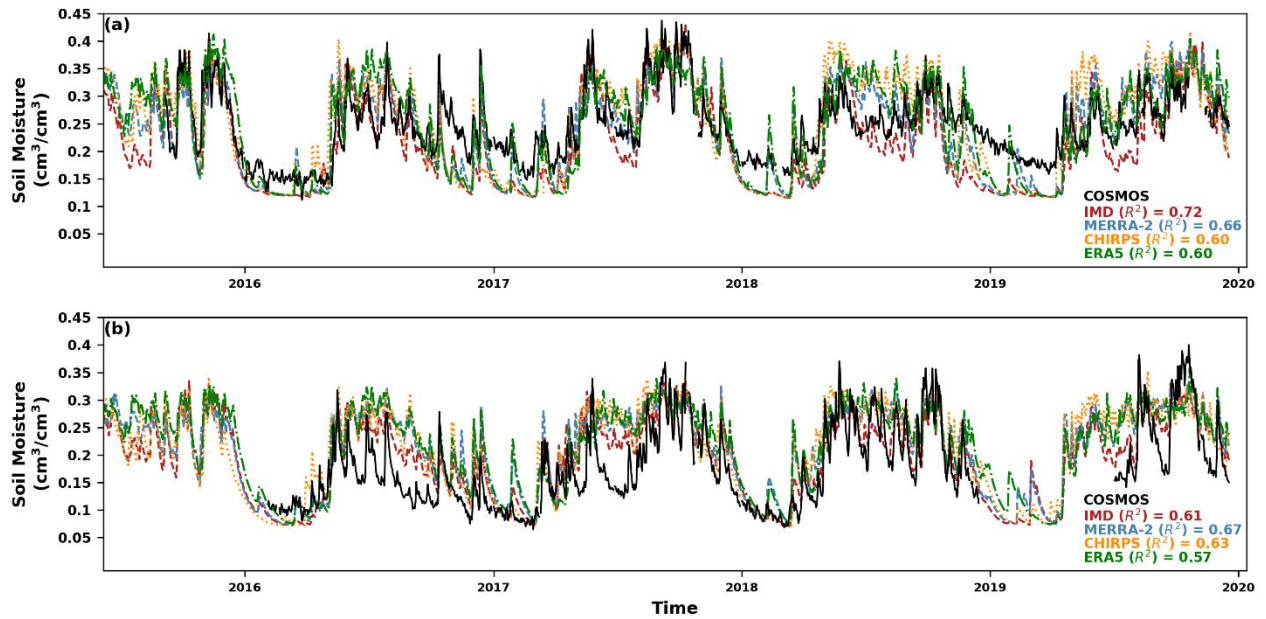
417 The in-situ soil moisture observations in India are rare due to sparse gauge network and
 418 limited data availability. The validation with in-situ COSMOS soil moisture observations was
 419 performed at daily and monthly scale for a period of 2015-2019 at two-gauge stations. The

420 monthly simulated soil moisture shows good agreement with in-situ soil moisture data
 421 throughout the time series as the R^2 is greater than 0.66 at both gauge stations for all four
 422 meteorological forcing (Fig. 5). The model retains skill at daily scale as R^2 varies from 0.74
 423 to 0.68 and 0.61 to 0.57 at SGR and MDH, respectively (Fig. 6). We also evaluated basin-
 424 wise trend and found that the simulated and ESA-CCI soil moisture anomaly do not show
 425 significant trend in most of the basins at monthly scale (Fig. S1).



426

427 *Fig. 5. Comparison of simulated monthly mean soil moisture for different meteorological*
 428 *forcings (IMD, MERRA-2, CHIRPS, and ERA-5) with COSMOS (in-situ) soil moisture at*
 429 *two-gauge stations (a) SGR and (b) MDH from June 2015 to December 2019.*



430

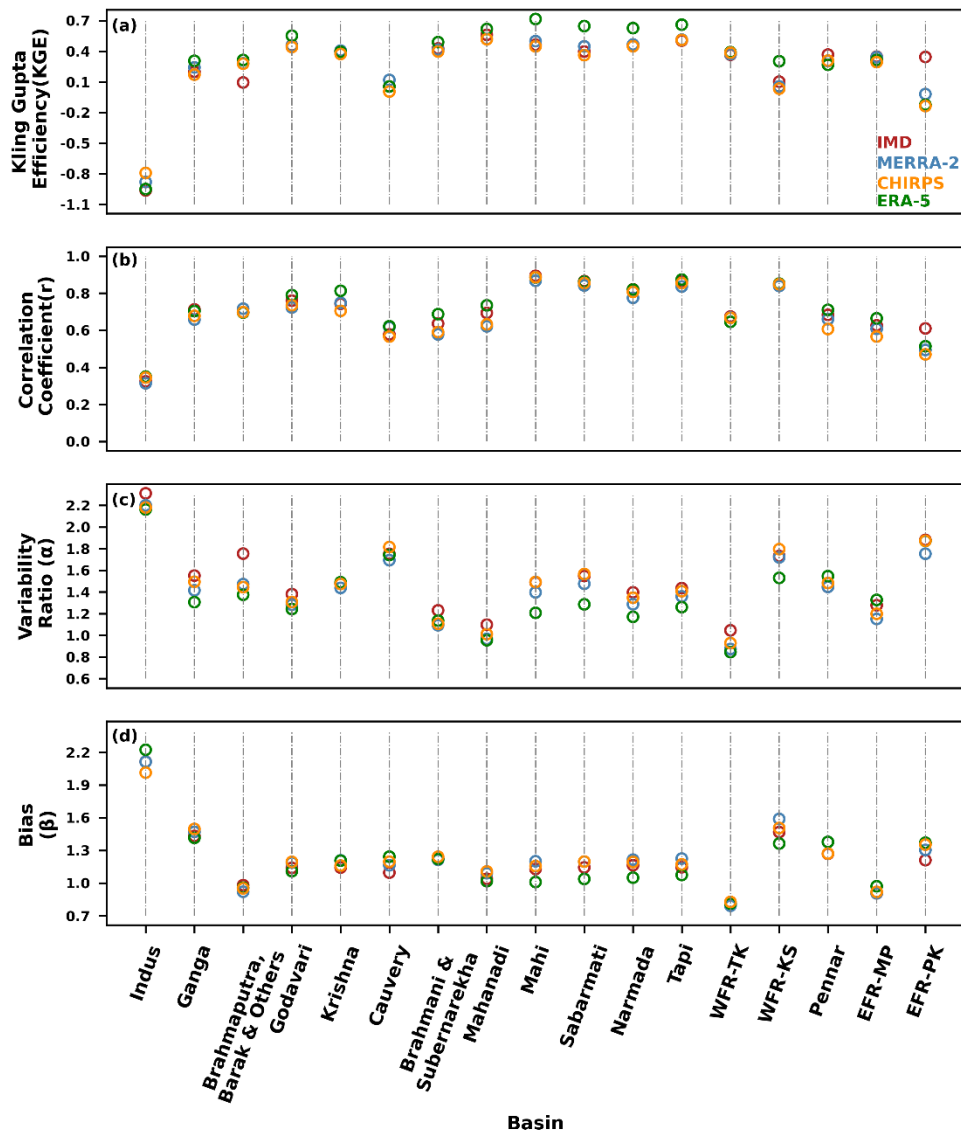
431 *Fig. 6. Comparison of simulated daily mean soil moisture for different meteorological*
 432 *forcings (IMD, MERRA-2, CHIRPS, and ERA-5) with COSMOS (in-situ) soil moisture at*
 433 *two-gauge stations (a) SGR and (b) MDH from June 2015 to December 2019.*

434

435 3.2.2. Evapotranspiration

436 We evaluated the ILDAS simulated evapotranspiration with the four meteorological
 437 forcings against the MODIS Aqua Evapotranspiration from 2002 to 2021 (Fig. 7). We
 438 calculated basin-wise KGE (Fig. 7a) and found that the ILDAS performs well in most of the
 439 basins except Indus, Cauvery, and east flowing rivers from Pennar to Kanyakumari. ERA-5
 440 shows a high basin-wise median r (Fig. 7b) in most of the basins than IMD, MERRA-2 and
 441 CHIRPS. Most of the basins show variability greater than one for evapotranspiration with all
 442 four meteorological forcings (Fig. 7c). However, Brahmaputra and west flowing rivers from
 443 Tapi to Kanyakumari show variability near to one than other basins (Fig. 7c). We found that
 444 all four meteorological forcings (IMD, MERRA-2, CHIRPS, and ERA-5) show
 445 overestimation in most of the basins except Brahmaputra, and west flowing rivers from Tapi
 446 to Kanyakumari (Fig. 7d). However, in an early study, Srivastava et al., (2017) stated that the

447 MODIS underestimated evapotranspiration in India; Our results show a higher bias in most of
 448 the basins. All four meteorological forcings show overestimation of the mean annual
 449 evapotranspiration compared to the MODIS aqua evapotranspiration (Fig. S2a). Most of the
 450 basins show a positive trend in simulated and MODIS aqua evapotranspiration except
 451 Brahmaputra, whereas CHIRPS shows a negative trend (Fig. S2b).

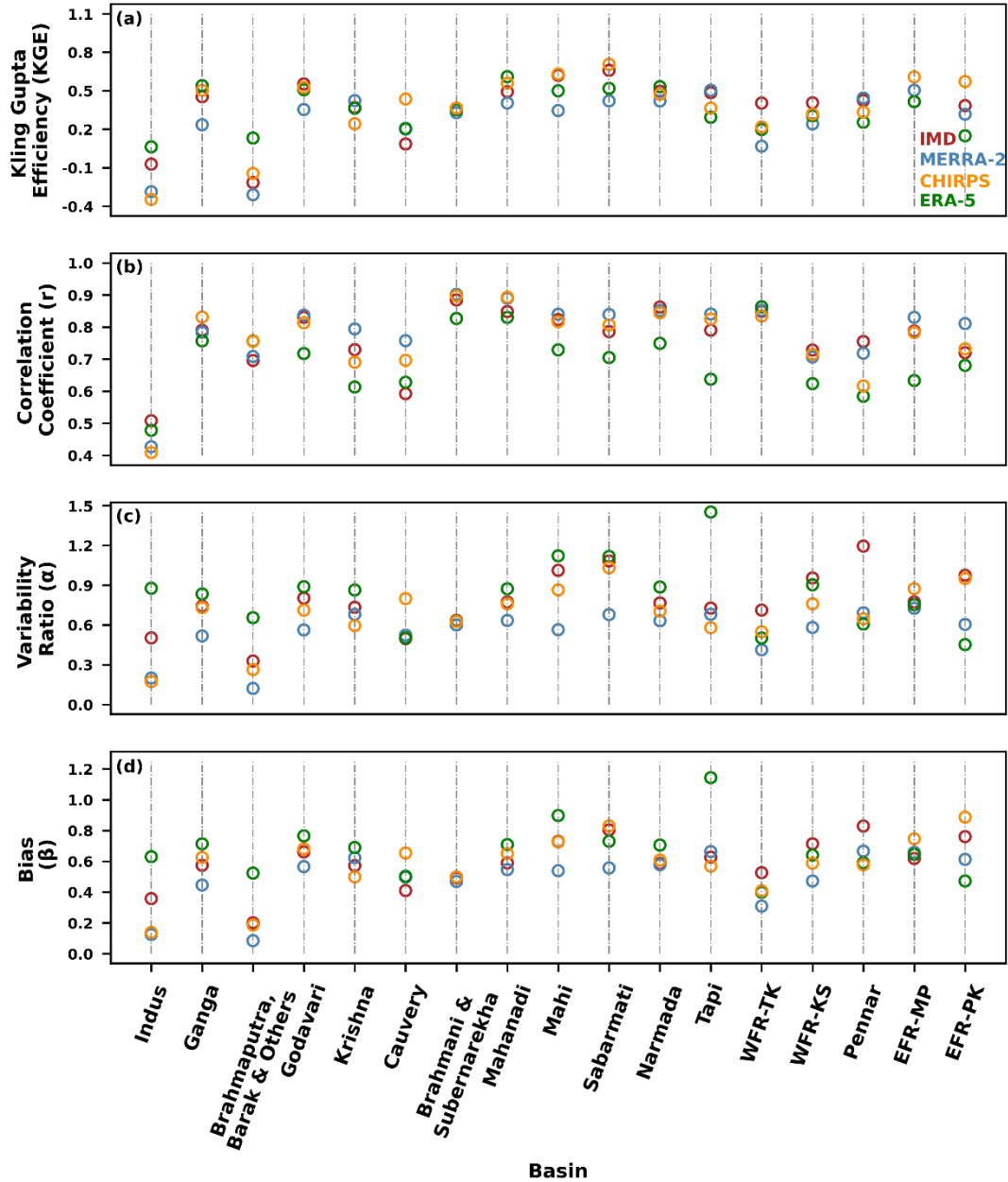


452

453 Fig. 7. Basin-wise comparison of KGE, correlation, α , and β of simulated monthly mean
 454 evapotranspiration for different meteorological forcing (IMD, MERRA-2, CHIRPS, and
 455 ERA-5) with MODIS Aqua (MYD16A2GF) Evapotranspiration product for 2002-2021.

456 3.2.3. Runoff

457 We evaluated simulated runoff for different meteorological forcings against GRUN
458 runoff (Fig. 8a-d). We found that all four meteorological forcings show poor performance
459 ($KGE < 0.2$) in the Indus and Brahmaputra River basins (Himalayan region) (Fig. 8a).
460 However, the ERA-5 performs better other three forcings in Indus and Brahmaputra. GRUN
461 (Ghiggi et al., 2019) did not consider glacier melting in the generation of runoff data and this
462 may lead to larger uncertainties in the Himalayan region, and our meteorological forcings
463 underestimated the precipitation in this region, which may incorporate the uncertainty in the
464 runoff. All four meteorological forcings show a high correlation in the Indian subcontinent
465 (Fig. 8b). However, the correlation is relatively less in the Indus and Himalayan regions
466 compared to other parts of India. Next, we checked the basin-wise variability of simulated
467 runoff from the model with all four meteorological forcings against the GRUN runoff (Fig.
468 8c). We found that variability in the runoff is less than one in the basins for all four
469 meteorological forcings except Tapi. However, ERA-5 and IMD show variability closer to
470 one compared to MERRA-2 and CHIRPS. We found that the runoff is highly underestimated
471 (Fig. 8d) in the Indus, Brahmaputra, and Western Ghats regions, possibly due to the hilly
472 terrains in these regions and the lack of incorporation of irrigation practices in our current
473 system. Irrigation leads to a decrease in runoff, which is currently underrepresented and will
474 be incorporated in the next version of the system. We found that all meteorological forcings
475 are underestimating the runoff (Fig. S3a). Next, we evaluated the basin-wise trend, all
476 meteorological forcings showed positive trend in most of the basins (Fig. S3b). Overall, IMD
477 performed better compared to MERRA-2, CHIRPS and ERA-5 in simulating runoff.



478

479 *Fig. 8. Basin-wise comparison of KGE, correlation, α , and β of simulated monthly mean*
 480 *Runoff for different meteorological forcings (IMD, MERRA-2, CHIRPS, and ERA-5) with*
 481 *monthly mean GRUN Runoff for 1981-2014.*

482 3.2.4. Streamflow

483 We calculated KGE and its components for simulated vs observed monthly
 484 streamflow from 1981-2021 for each gauge location. The spatial distribution of performance
 485 for all gauge stations on an annual basis is shown in (Fig. 9). Comparing the nationwide

486 median and interquartile range (IQR) of overall KGE score, IMD scored the highest median
487 value of 0.36 (IQR: 0.08 – 0.57), closely followed by CHIRPS and ERA-5 with median
488 values of 0.33 (IQR: 0.04 – 0.56) and 0.3 (IQR: -0.08 – 0.58), respectively. MERRA-2 scored
489 the lowest median value of 0.27 (IQR: 0.06 – 0.47). The west flowing rivers from Tapi to
490 Kanyakumari show the highest KGE scores, whereas the gauge stations in central India
491 exhibited majority of the underperformance (Fig. 9a-d). While comparing the performance of
492 individual KGE components, we found that all four forcings showed a good median
493 correlation ($r > 0.7$), with IMD scoring the highest nationwide median value of 0.83,
494 followed by ERA-5 (0.81), CHIRPS (0.75) and MERRA-2 (0.71). Additionally, 94% of
495 gauge stations had a $r \geq 0.5$ for ERA-5, 92% for IMD, 89% for CHIRPS, and 79% for
496 MERRA-2. It may be noted that even though the median correlation for ERA-5 is lower than
497 IMD, it shows correlation greater than 0.5 in more basins compared to IMD. The spatial
498 distribution of gauge stations with high r scores matches with those that had high overall
499 KGE scores, with most of the underperformance seen in upper Ganga River basin (Fig. 9e-h)
500 as multiple reservoirs and other irrigation structures result in a delayed response in the river's
501 streamflow. In terms of statistical variability of monthly flows, IMD, CHIRPS and ERA-5
502 had $\alpha > 1$ in most gauge stations (51%, 52% and 61%, respectively), which corresponds to
503 higher variability in simulated values as compared to the observed ones. In contrast,
504 MERRA-2 showed low variability with $\alpha < 1$ in 63% of the gauge stations. In terms of the
505 spatial distribution, the relatively lower values of α are seen majorly in Ganga River basin
506 and some of the gauge stations in west flowing rivers. However, for ERA-5 simulations, the
507 variability in Ganga River basin is higher than the observed, which also resulted in the
508 highest overall median α (1.08). The nationwide median β was lowest for MERRA-2 (1.11),
509 followed by IMD (1.13), CHIRPS (1.15) and ERA-5 (1.4). All forcings showed positive bias
510 in simulated streamflow for most of the stations with ERA-5 showing highest number of
511 gauge stations with overestimated streamflow (70%), followed by CHIRPS (61%), IMD

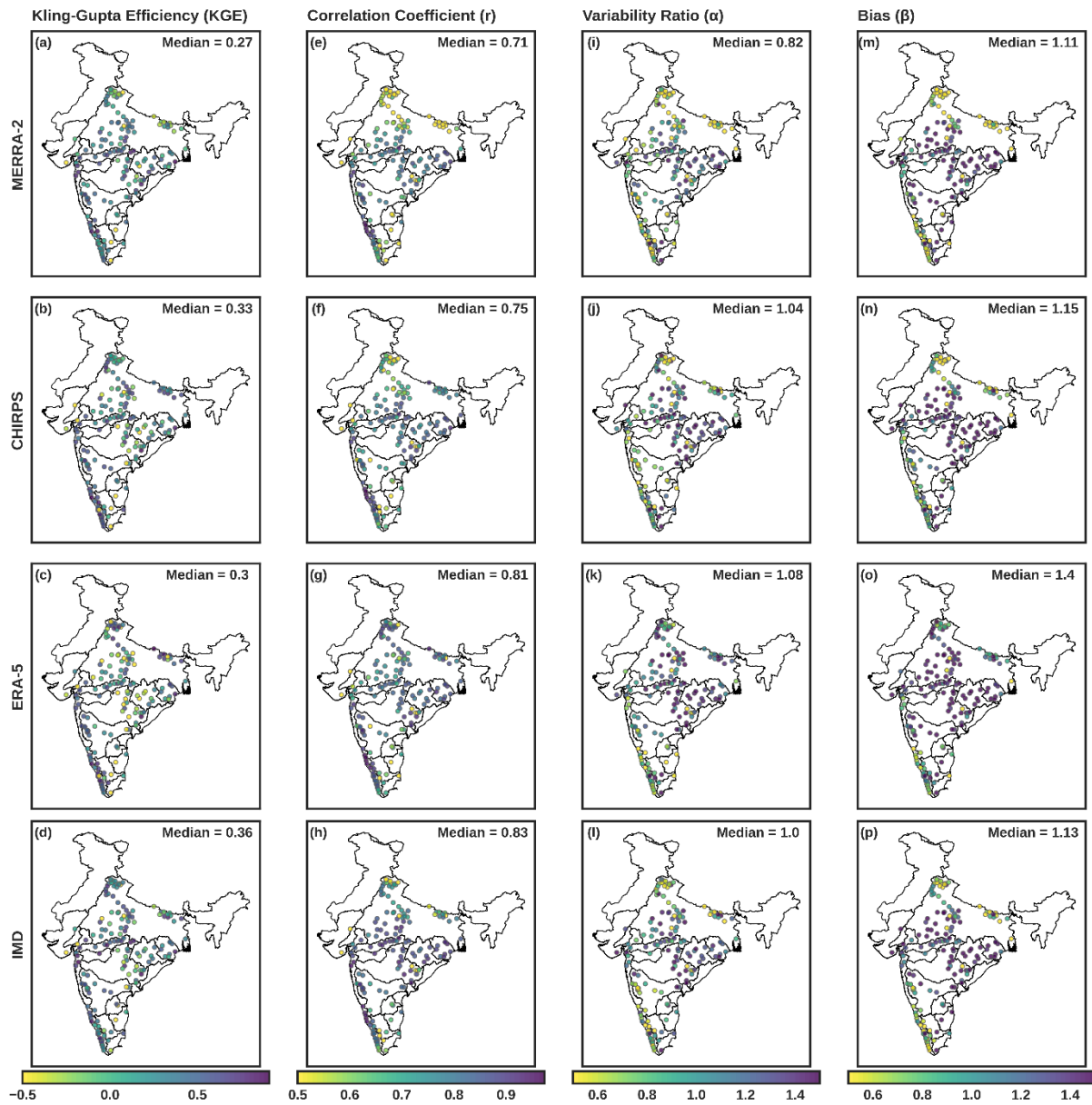
512 (59%) and MERRA-2 (53%). Additionally, we also found that ERA-5 had the highest
513 number of gauge stations (20%) with a bias greater than 100% ($\beta \geq 2$), compared to CHIRPS
514 (12%), IMD (9%) and MERRA-2 (4%). The high median β for streamflow simulated by
515 ERA-5 and CHIRPS shows that the ILDAS struggled to match the magnitude of seasonal
516 flows, especially in the central and peninsular regions which is expected due to the non-
517 perennial rivers and various anthropogenic activities (Fig. 9m-p). Overall, IMD can be
518 considered as the best performing precipitation forcing among the four based on median KGE
519 value.

520 Besides annual evaluation, since most of the precipitation over India is concentrated in the
521 months of June-September (also known as JJAS season) which results in very high seasonal
522 flows in the Indian rivers, we also evaluated the simulated streamflow specifically for JJAS
523 season (Fig. 10). Overall, the nationwide KGE median score increased by 11.1% for
524 MERRA-2 and IMD) and 6.6% for ERA-5 (0.32 vs 0.3) but decreased for CHIRPS by 6%
525 (0.33 vs 0.31). However, all four forcings saw a reduction of in median r score in JJAS
526 season, with values of 0.62, 0.64, 0.71, 0.77 for MERRA-2, CHIRPS, ERA-5 and IMD,
527 respectively. Additionally, a corresponding reduction in β is observed, while α decreased
528 marginally for CHIRPS but increased for MERRA-2, ERA-5 and IMD. Hence, during the
529 JJAS season, ILDAS captured the magnitude and variability of high monsoon flows with a
530 higher skill, but the timing could not be matched well, which is due to the various regulatory
531 structures such as reservoirs resulting in a reduced as well as delayed streamflow in the
532 rivers.

533 The performance of the integrated hydrological-hydrodynamic model can be assessed by
534 evaluating the overall patterns of streamflow. Therefore, we calculated monthly streamflow
535 anomalies for all four forcings and compared them against the observed to assess the ability
536 of ILDAS to capture general streamflow patterns during the annual cycle and monsoon
537 season. We used the anomaly correlation coefficient and unbiased RMSE (ubRMSE) to

538 evaluate the performance of the model across 162 catchments (Fig. 11-12). The results of the
539 annual evaluation showed that the IMD driven streamflow had the highest correlation with
540 the observed anomalies (0.69), followed by ERA-5 (0.57), MERRA-2 (0.53), and CHIRPS
541 (0.51). Although the anomaly correlation coefficient marginally improved during the JJAS
542 season, the ubRMSE showed a significant increase in value across all forcings, suggesting
543 that ILDAS overestimated the anomalies during the monsoon (Fig. 12e-h). This could be due
544 to the lack of information regarding various management practices, such as reservoirs, in
545 ILDAS which caused the model to simulate higher flows than observed. The overall superior
546 performance of IMD could be due the localized and more accurate precipitation information
547 as it leverages the extensive network of rain gauges across India.

548 On the daily scale, daily streamflow shows a nationwide median KGE of 0.27, compared
549 to 0.36 for IMD monthly. The error metrics for other meteorological forcings are presented in
550 Figure S5-S6. The assessment of daily streamflow anomaly correlation for annual season
551 shows that IMD has highest correlation with observed anomalies ($R = 0.48$), followed by
552 ERA-5 (0.36), CHIRPS (0.31), and MERRA2 (0.29). For JJAS season, the daily anomaly
553 correlation largely remains same but ubRMSE increases significantly, indicating higher
554 variability in daily monsoon flows (Fig.13). The skill of streamflow simulations at daily scale
555 emphasizes the future need for calibration and including anthropogenic effects into the model
556 such as reservoirs. To further investigate the performance of ILDAS, we also calculated
557 commonly used hydrological signatures such as mean annual flow, mean annual monsoon
558 flow, low flow, and high flow. Using the coefficient of determination (R^2) as the performance
559 metric, we observed that ERA-5 had the highest R^2 scores across all hydrological signatures
560 followed by CHIRPS, IMD, and MERRA-2 (Fig. 14). The highest and lowest R^2 scores were
561 observed for mean annual high flow and mean annual low flow, respectively. The low R^2 for
562 mean annual low flows emphasizes the need for incorporating the anthropogenic effects and
563 calibration of the model.

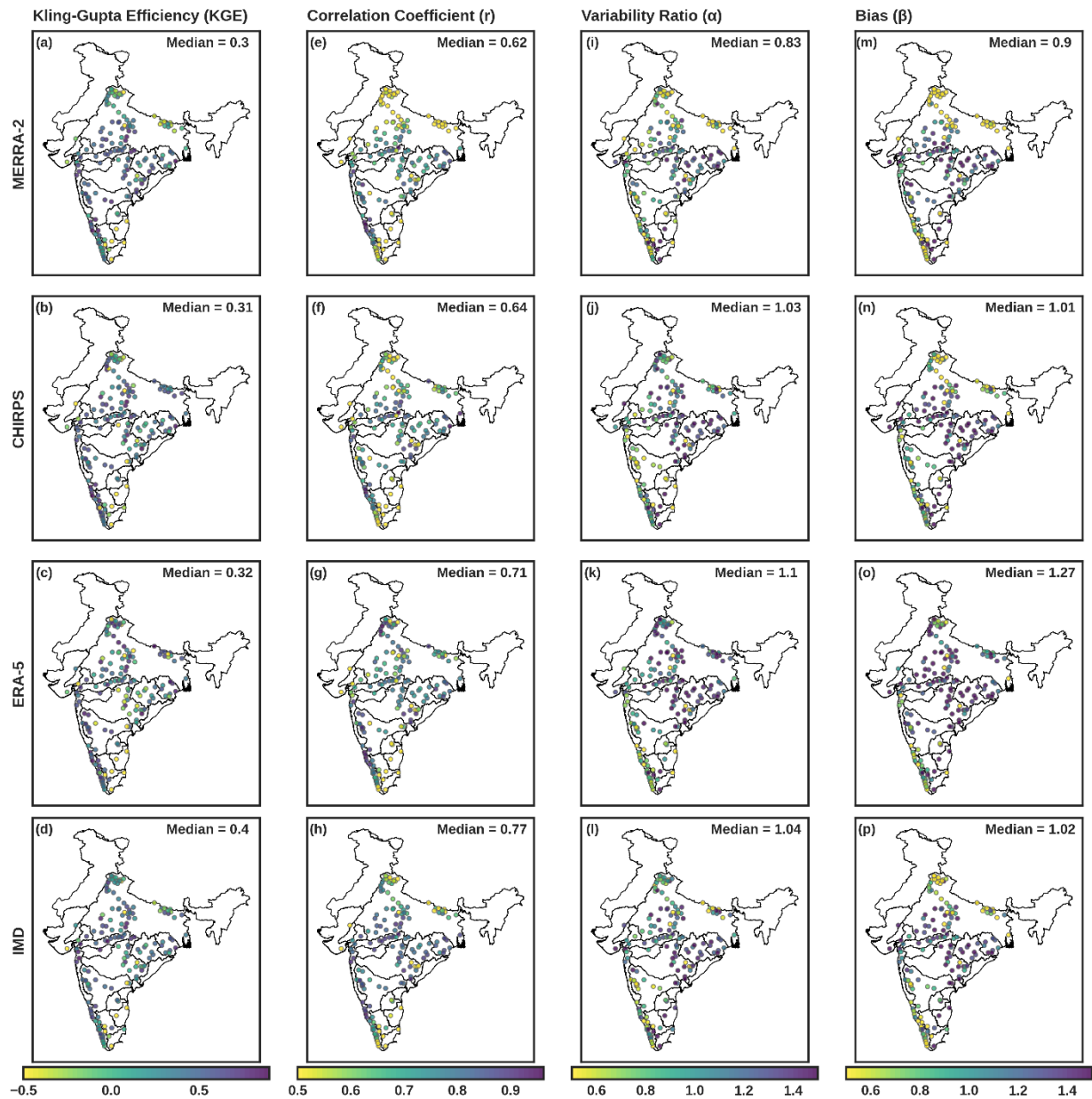


564

565

566

Fig. 9. Comparison of KGE (a-d), r (e-h), α (i-l), and β (m-p) of simulated monthly mean streamflow annually for different meteorological forcings at 162 gauge stations.



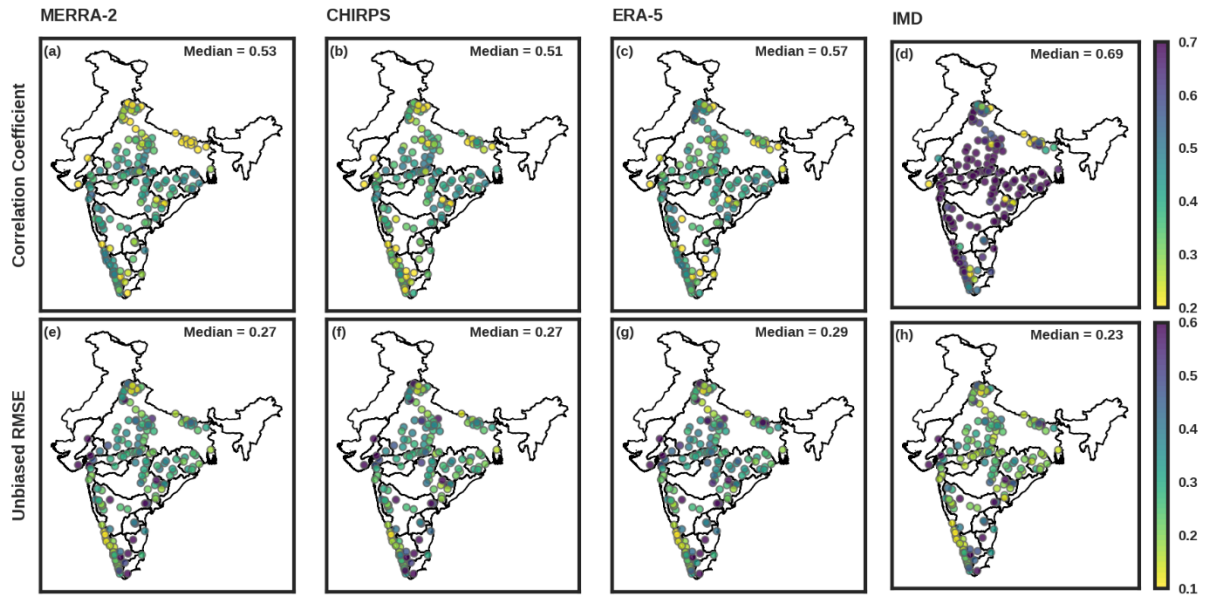
567

568 *Fig. 10. Comparison of KGE (a-d), r (e-h), α (i-l), and β (m-p) of simulated monthly mean*
 569 *streamflow in JJAS season for different meteorological forcings at 162 gauge stations.*

570 Table 5. Detailed analysis of monthly simulated streamflow against observed streamflow for
 571 annual and JJAS (monsoon season) from 1981-2019 for the four forcings. The digits
 572 represent the number of gauge stations (out of 162) falling under the specified criteria.

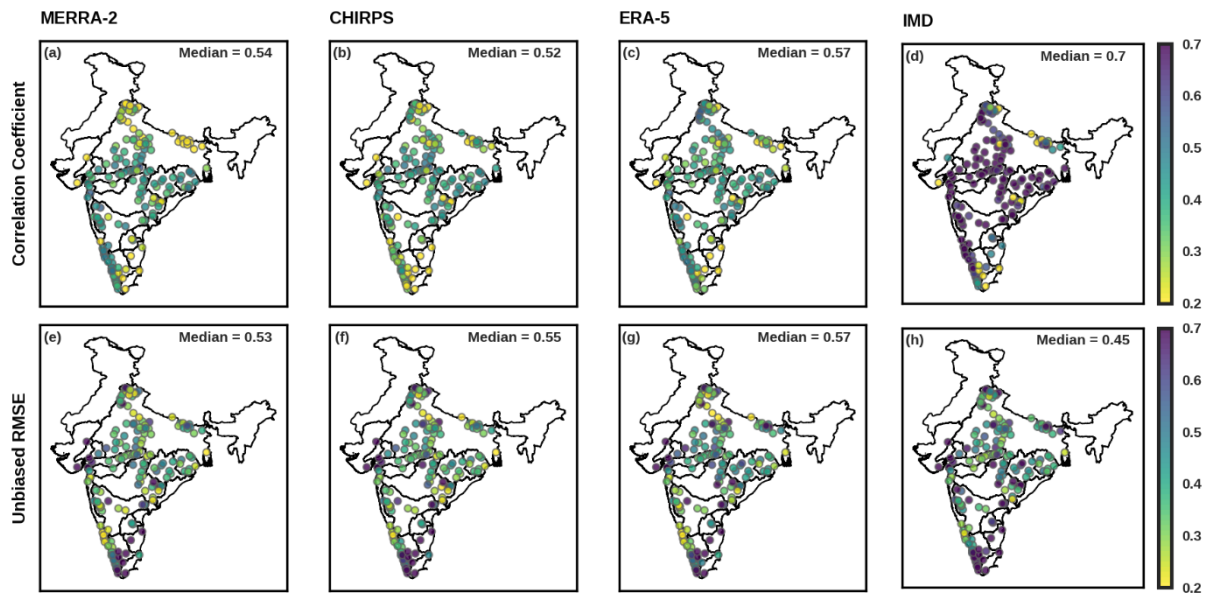
Criteria	MERRA-2	CHIRPS	ERA-5	IMD
----------	---------	--------	-------	-----

	Annual	JJAS	Annual	JJAS	Annual	JJAS	Annual	JJAS
KGE								
Inter	0.06 -	0.01 -	0.04 -	0.11 -	-0.08 -	0.02 -	0.08 -	0.1 - 0.59
Quartile	0.47	0.51	0.56	0.49	0.58	0.52	0.57	
Range								
Correlation								
(r)								
Distribution	128/34	113/49	144/18	129/33	152/10	142/20	147/15	135/27
(>=0.5/<0.5)								
Variability								
(α)								
Distribution	103/59	101/61	78/84	78/84	64/98	71/91	80/82	73/89
(low/high)								
Bias (β)								
Distribution								
(negative/positive)	76/86	86/76	63/99	80/82	49/113	54/108	57/95	78/84
β >= 2	7	6	19	9	32	16	14	7



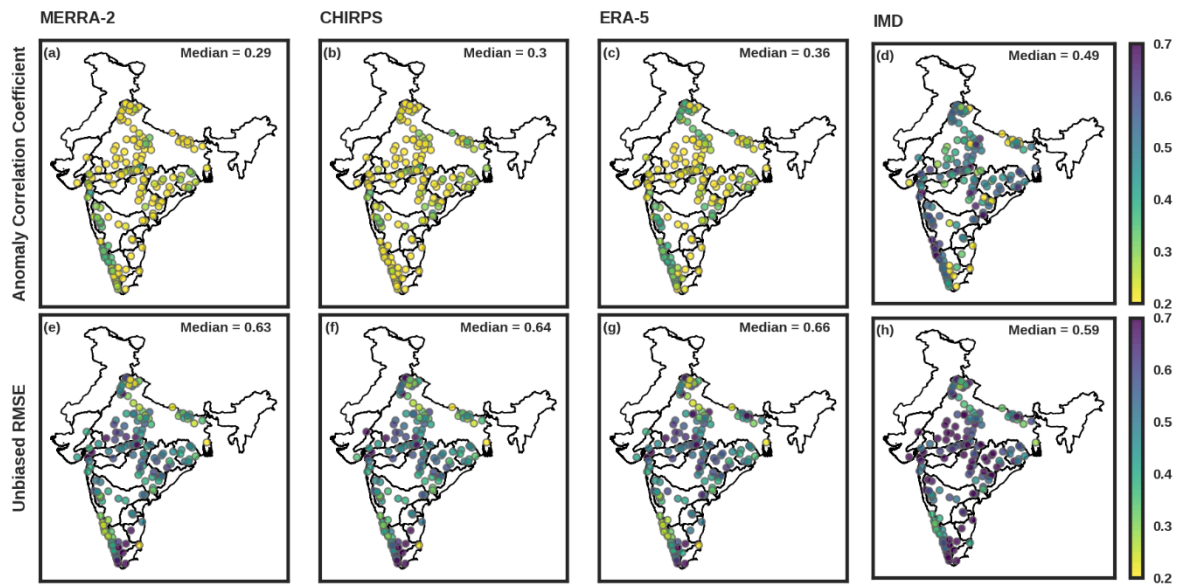
573

574 *Fig. 11. Anomaly correlation coefficient (a-d) and unbiased RMSE (e-h) for monthly mean*
 575 *streamflow in annual season for different meteorological forcings at 162 gauge stations.*



576

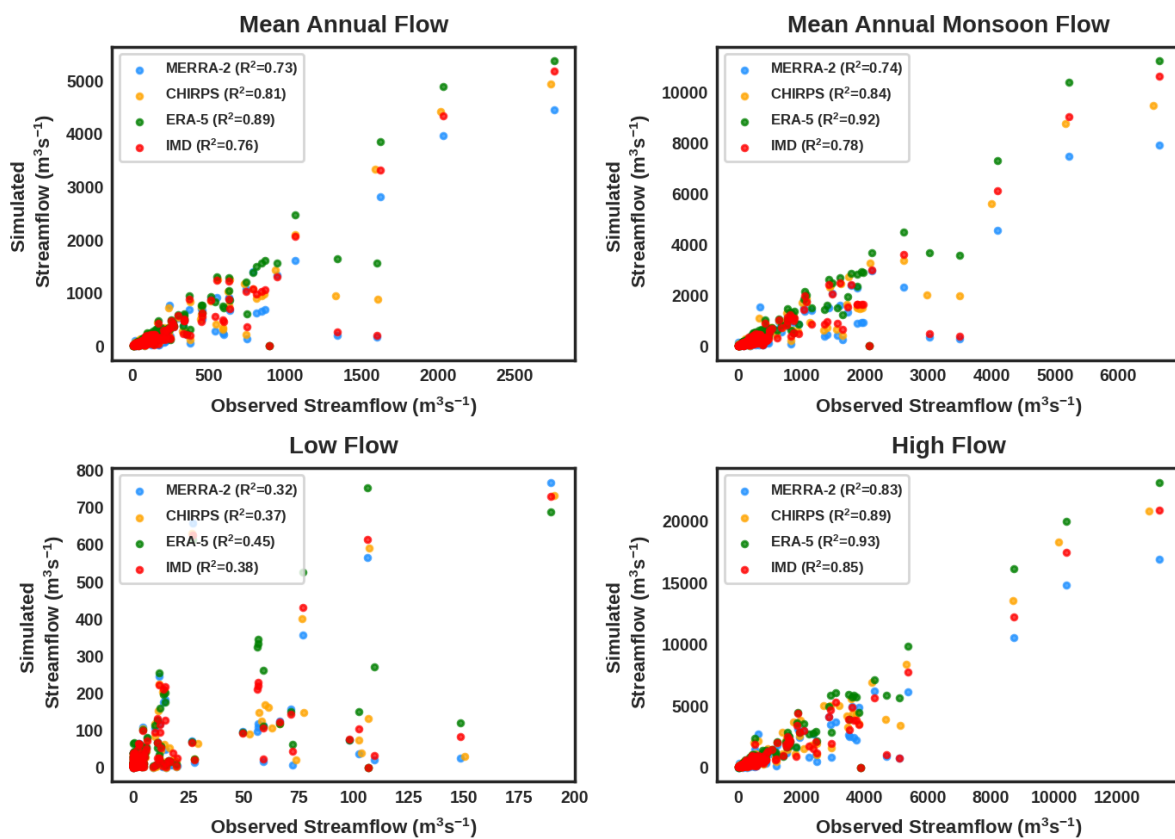
577 *Fig. 12. Anomaly correlation coefficient (a-d) and unbiased RMSE (e-h) for monthly mean*
 578 *streamflow in JJAS season for different meteorological forcings at 162 gauge stations.*



579

580 Fig. 13. Anomaly correlation coefficient (a-d) and unbiased RMSE (e-h) for daily streamflow

581 in JJAS season for different meteorological forcings at 162 gauge stations.



582

583 Fig. 14. Scatter plots of various hydrological signatures for 162 catchments across Indian

584 subcontinent. The values in-set denote coefficient of determination (R^2) corresponding to

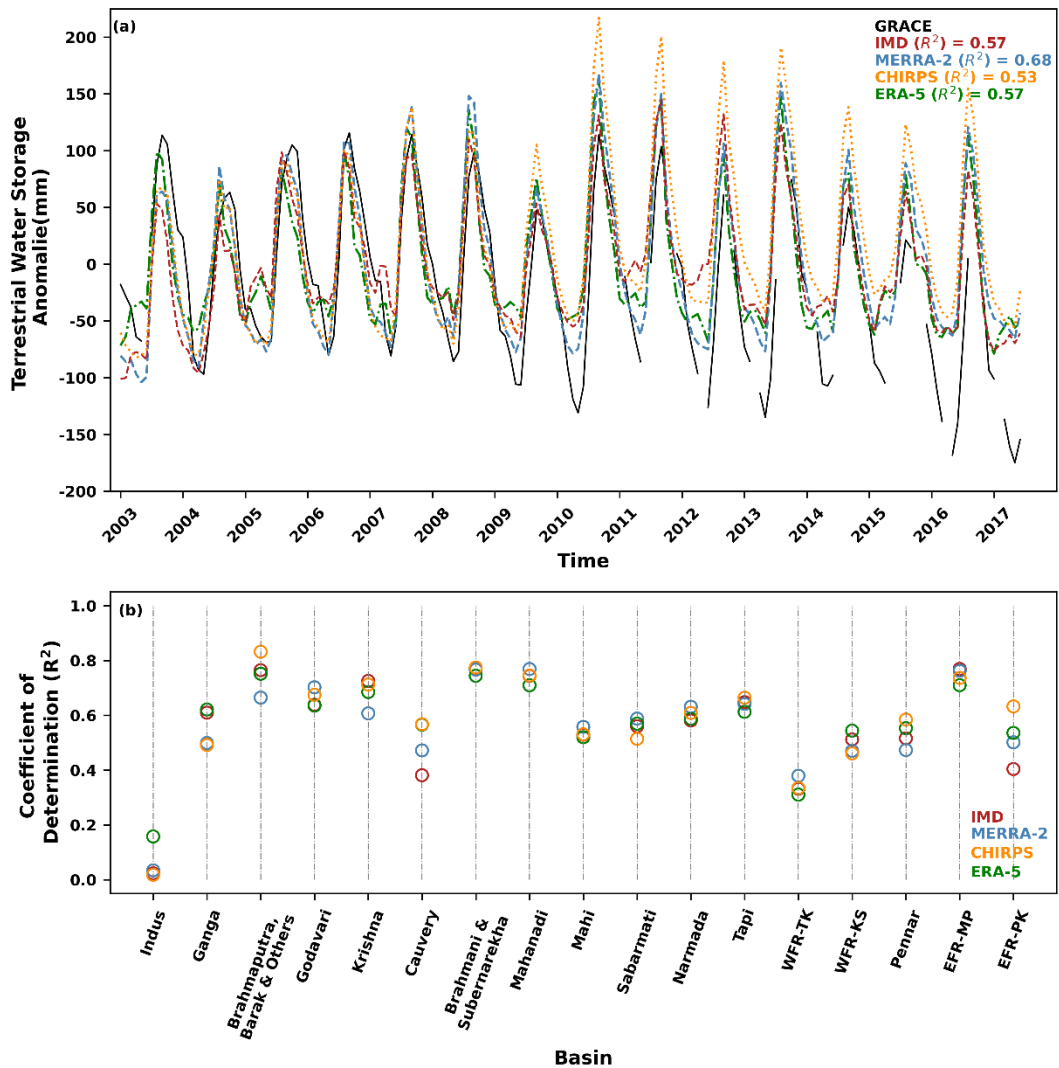
585

each hydrological signature.

586 3.2.5. Terrestrial Water Storage Anomaly (TWSA)

587 We evaluated the TWS for all meteorological forcings by adding Land Surface Model (LSM)
588 water storage (LWS) and Surface water storage (SWS). LWS consists of groundwater storage
589 (GWS), soil moisture (SM), and snow water equivalent (SWE). Most of the studies do not
590 consider the SWS in the TWS. However, Surface water storage (SWS) contributes 8% of
591 TWS variability globally (A. Getirana, Kumar, et al., 2017). While comparing the time series
592 of nationwide monthly mean simulated TWSA using Noah MP + HyMAP with
593 meteorological forcings to GRACE TWSA for 2003-2017 (Fig. 15a), we found that all four
594 meteorological forcings had captured the seasonality of TWSA well. However, from 2010
595 onward, all meteorological forcings overestimated the peaks and the troughs. We noted that
596 GRACE shows a negative trend in the TWSA. This negative trend may be due to the
597 extensive extraction of groundwater in parts of India such as Punjab, East Flowing River
598 (Pennar-Kanyakumari) (EFR-PK) and Ganga basin. Similar patterns were observed by
599 previous studies in the Indian mainland (Satish Kumar et al., 2023). We found that CHIRPS
600 shows a positive trend, whereas IMD, MERRA-2, and ERA-5 show relatively no trend.
601 Uncertainties in the TWSA GRACE and ILIAS simulated TWSA may be due to India's
602 anthropogenic conditions and irrigation, which will be incorporated in ILIAS in the future.
603 We also calculated the basin-wise R^2 for the primary basin and found that most of the basins
604 show high R^2 for MERRA-2 and ERA-5 (Fig. 15b). Moreover, all forcings show poor R^2 in
605 the Indus River basin which could be due to the excessive groundwater extraction in this
606 region. Previous studies (Asoka & Mishra, 2020; Maina et al., 2022) have also shown a
607 similar pattern in the northwest (Indus) region. Overall, our results show that IMD, MERRA-
608 2, and ERA-5 performed well with a nationwide mean ($R^2 > 0.57$) except CHIRPS ($R^2 =$
609 0.53). Similarly, Soni and Syed, (2015) also found similar performance in the major river
610 basins of India.

611



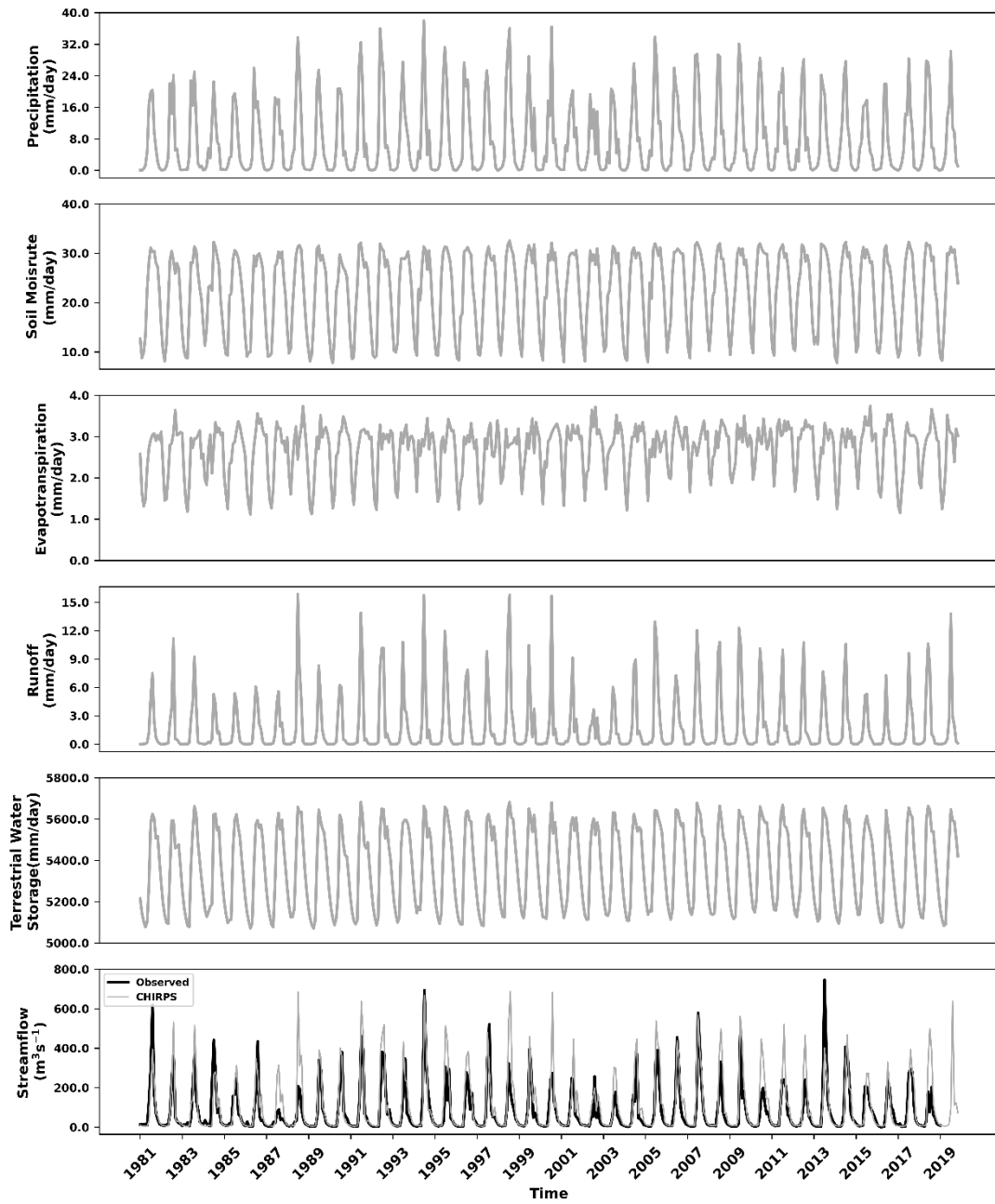
612

613 *Fig. 15. A plot of time series plot for nationwide monthly mean terrestrial water storage*
 614 *anomaly for GRACE, IMD, MERRA-2, CHIRPS, and ERA-5 for 2003-2017 (a) and basin-*
 615 *wise R^2 (b).*

616 3.2.6. Seasonal Water Balance Cycle

617 A coupled hydrological-hydrodynamic model is expected to capture the variation of
 618 long-term water balance of the region. Therefore, along with the quantitative assessment of
 619 water balance components discussed in the previous sections, we've tried to illustrate the
 620 ability of ILDAS in capturing the seasonal variation of the terrestrial water budget using time
 621 series plots of various water balance components along with the anomalies of water fluxes

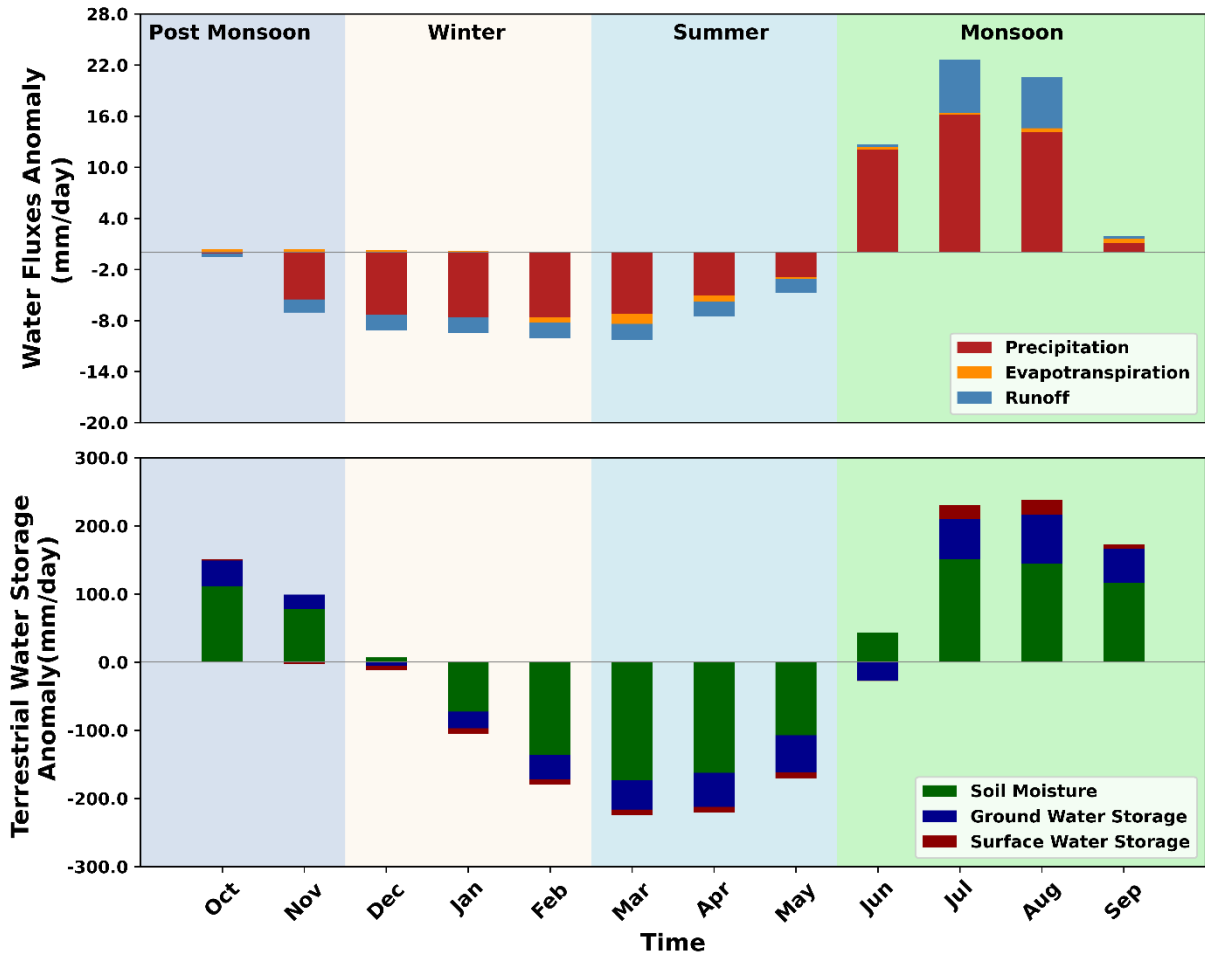
622 and the terrestrial water storage. Here, we present the qualitative analysis for simulated water
623 balance using CHIRPS at Kudige, Cauvery River basin, which is a rain-fed region in the
624 southern India (Fig. 16-17). Fig. 16 shows the long-term variation of various water balance
625 components for the period 1981-2021. Additionally, Fig. 17 shows the monthly anomalies for
626 simulated water balance for four different meteorological seasons. We observed that ILDAS
627 is successful in simulating the long-term seasonal variation in terrestrial water storage with
628 precipitation as the primary factor. The terrestrial water storage remains in deficit compared
629 to long term monthly mean when precipitation is low in winters and summers, followed by a
630 surplus period in monsoons, which agrees with the climate and topography of the basin.
631 Moreover, the deficit is largest during the peak summer which gets replenished in the
632 subsequent monsoon.



633

Fig. 16. A time-series plot showing long-term variation of various components of simulated water balance at Kudige, Cauvery River basin.

634

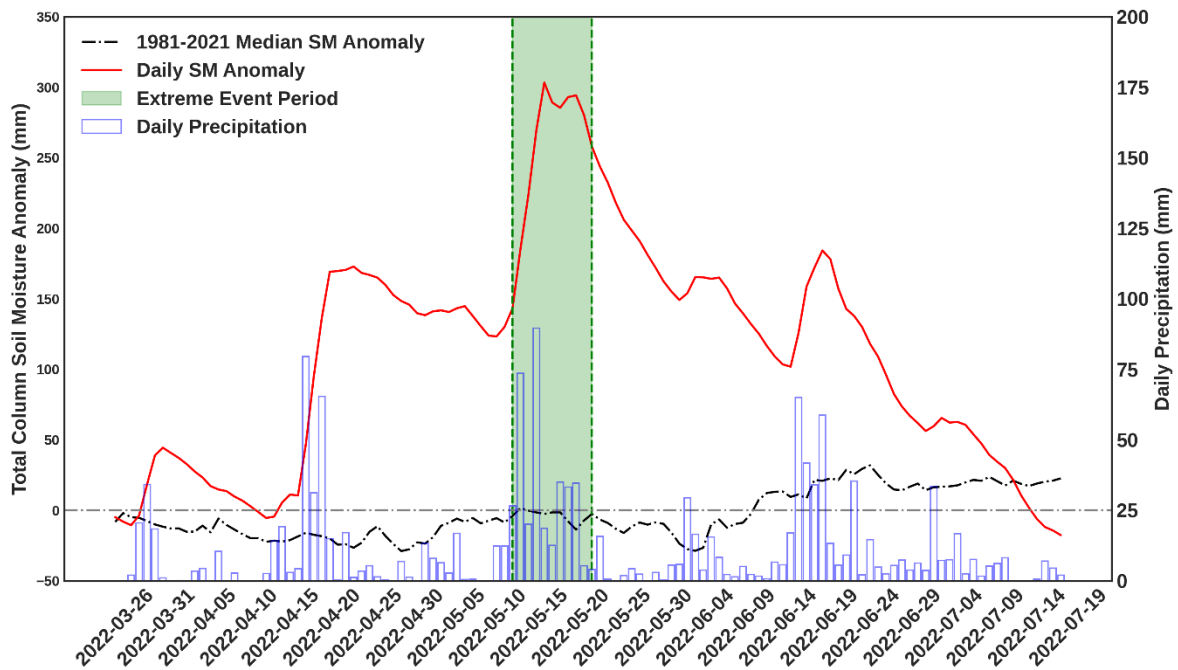


635 Fig. 17. Seasonal variations of different water balance components as monthly anomalies
 636 simulated using ILDAS forced by CHIRPS at Kudige, Cauvery River basin.

637 3.2.8 Hydroclimatic Extreme Event Analysis

638 In May 2022, the town of Haflong, located in the Dima Hasao district of Assam,
 639 India, experienced a catastrophic series of landslides and floods resulting in extensive
 640 damage and loss of life and property. The disaster occurred between May 11-18 and was
 641 triggered by heavy rainfall, affecting multiple villages in the area (Roy et al., 2023). The
 642 landslides caused severe damage to infrastructure such as roads, bridges, and buildings,
 643 hampering rescue and relief efforts. To better understand the underlying conditions, we
 644 reconstructed the total column soil moisture (1000 mm) in the area from 1981-2022 and
 645 compared the 2022 daily soil moisture anomaly to 1981-2021 median (Fig. 18). Fig. 18

646 illustrates that the antecedent soil moisture anomaly in the area was significantly higher than
647 the long-term median, indicating saturation of the soil due to heavy rainfall on April 15-17.
648 This heightened soil moisture content increased the vulnerability to landslides and
649 inundation. The subsequent high rainfall in May resulted in high runoffs and increased pore
650 pressure which caused district wide inundation and cluster landslides due to slope failure at
651 multiple sites. This finding underscores the importance of monitoring soil moisture
652 conditions and incorporating this information into landslide risk assessment and management
653 strategies. The ILDAS was able to capture the local antecedent soil moisture condition even
654 at an uncalibrated stage which is a promising prospect for future implementation in
655 operational forecasts.



656

657 *Fig. 18. Reconstructed daily soil moisture anomaly in Haflong, Assam for the extreme*
658 *hydroclimatic event that occurred from 11-18 May 2022.*

659

660 4. Conclusions

661 We have established ILDAS as a prototype of a coupled hydrologic-hydrodynamic
662 system to generate a high-quality reanalysis of land surface estimates and streamflow at 0.1°
663 resolution and daily temporal resolution across the Indian mainland for the period 1981-2021.
664 We tested the ILDAS using three meteorological forcings with varying spatial and temporal
665 resolutions and assessed its ability to simulate various water balance components such as soil
666 moisture, evapotranspiration, surface runoff, streamflow, and terrestrial water storage
667 anomalies. We evaluated the uncertainty and bias in the precipitation component of three
668 global meteorological forcings across the various regions of India. We found that CHIRPS
669 exhibits lower uncertainty than MERRA-2 and ERA-5, and a high correlation and minimum
670 RRMSE against observation-based IMD precipitation. Additionally, we evaluated all major
671 components of simulated water balance. It was found that all meteorological forcings showed
672 good performance for simulated soil moisture by ILDAS. However, MERRA-2 showed
673 minimum median ubRMSE value for most of the basins compared to others. The correlation
674 is high in simulated soil moisture as well as runoff for all meteorological forcings. However,
675 our results did not indicate good agreement with GRUN runoff in the Himalayan region,
676 which may be due to glacier melting not being considered in generating GRUN runoff. We
677 evaluated the average monthly streamflow against observed streamflow at multiple gauge
678 stations for annual and the monsoon (JJAS) season. The overall results from the annual
679 evaluation show that ILDAS could match the streamflow timing better than the magnitude
680 and variability, especially in central and peninsular India, which may be caused by very low
681 flows during the non-monsoon months in seasonal rivers, that are further reduced due to
682 human abstractions. However, while evaluating the streamflow specifically during the
683 monsoon months, we found that the overall nationwide median values of both r and β were
684 reduced. This means that although ILDAS performance improved in capturing the magnitude
685 of streamflow, the timings of the flows could not be matched well. However, an overall
686 nationwide KGE of 0.36 for IMD in annual evaluation is a promising result for ILDAS,

687 which can be further improved using data assimilation, calibration, or post-processing. The
688 evaluation of monthly streamflow anomalies for annual season agreed with the evaluation of
689 streamflow timeseries and IMD showed highest anomaly correlation coefficient and lowest
690 ubRMSE. However, ubRMSE degraded for all the forcings in JJAS season due to the
691 uncalibrated state of ILDAS, resulting in higher than observed flows. While evaluating the
692 streamflow-derived hydrological signatures, we observed that IMD's superior performance in
693 simulating temporal patterns of streamflow did not translate to overall statistical streamflow
694 patterns of the catchments. The global forcings including ERA-5 and CHIRPS performed
695 better in simulating the hydrological signatures compared to IMD. The overall evaluation of
696 water balance components suggests that different meteorological forcings performed better
697 for different land surface variables, which highlights the value of developing an ensemble of
698 model configurations with multiple data sources. We also reconstructed antecedent soil
699 moisture during a recently occurred hydro-climatic extreme in Haflong town of Assam, India,
700 causing a series of landslides and inundation in the area. We observed that ILDAS
701 successfully simulated the observed daily soil moisture anomaly, which was significantly
702 higher before the extreme precipitation that occurred in May. This highlights the importance
703 of a high resolution hydrological-hydrodynamic model, such as ILDAS, for risk assessment
704 and disaster mitigation of hydro-climatic extremes.

705 This study is envisioned as a proof-of-concept of an integrated system over an underserved
706 region such as the Indian subcontinent as most land surface models run in uncoupled mode
707 with river routing models. The ILDAS will serve as a testbed for future experiments on
708 assimilating remote sensing observations and provide near real-time estimates of land surface
709 states, natural water balance, and energy fluxes that are consistent across space and time, with
710 the potential to assist policymakers in decision-making related to food security, water
711 resources management, mitigation of natural hazards, and assessing climate change impacts.
712 Furthermore, there is a pressing need for a transboundary water modeling system which can

713 be used by countries to assess inflows and outflows from the Ganga and Brahmaputra,
714 leading to better cooperation within South Asia in the water sector. The first version of
715 ILDAS has some limitations that will serve as the basis for future improvements. Currently,
716 ILDAS outputs are based on a "natural" terrestrial state, as no information regarding
717 irrigation and reservoirs has been incorporated. Moreover, we acknowledge the limitations of
718 simplified assumptions and inaccuracies in parameterization while representing the physical
719 processes. Future enhancements to ILDAS will include data assimilation of remote sensing
720 products, localized land use/land cover parameters, and representation of reservoirs.

721 **Acknowledgements**

722 This research was conducted in the HydroSense lab (<https://hydrosense.iitd.ac.in/>) of IIT
723 Delhi and the authors would like to gratefully acknowledge IIT Delhi High Performance
724 Computing facility for providing computational and storage resources. Dr. Manabendra
725 Saharia gratefully acknowledges financial support for this work from ISRO Space
726 Technology Cell (RP04139). He also acknowledges the MoES Monsoon Mission III
727 (RP04574); IC-IMPACTS (RP04558); and the Coalition for Disaster Resilient Infrastructure
728 (CDRI) Fellowship (RP04569) for continual support for the project. The authors thank Prof.
729 Sekhar Muddu (IISc) and Ms. Deepti Upadhyay for giving access to COSMOS soil moisture
730 data. The authors gratefully acknowledge the Central Water Commission (CWC), National
731 Water Informatics Centre, and the Ministry of Jal Shakti (MoJS) for providing the streamflow
732 datasets used in this study. The authors also acknowledge ISRO NRSC for providing access
733 to the 1:50000 LU/LC dataset.

734 **Compliance with Ethical Standards**

735 The authors declare that they have no conflict of interest.

736 **Data Availability Statement.**

737 The datasets used in this study are available from the following sources:

- 738 • IMD precipitation: https://www.imdpune.gov.in/Clim_Pred_LRF_New/
- 739 • Streamflow: Centra Water Commission, India, and India WRIS,
740 <https://indiawris.gov.in/wris/>
- 741 • MERRA-2: GMAO, NASA Goddard Space Flight Centre,
742 <https://disc.gsfc.nasa.gov/datasets?project=MERRA-2>
- 743 • CHIRPS: Climate Hazards Centre, UC Santa Barbara,
744 <https://data.chc.ucsb.edu/products/CHIRPS-2.0/>
- 745 • ERA-5: ECMWF, [https://www.ecmwf.int/en/forecasts/datasets/reanalysis-](https://www.ecmwf.int/en/forecasts/datasets/reanalysis-datasets/era5)
746 [datasets/era5](https://www.ecmwf.int/en/forecasts/datasets/reanalysis-datasets/era5)
- 747 • GRUN Runoff: Institute for Atmospheric and Climate Science, ETH Zurich,
748 https://figshare.com/articles/dataset/GRUN_Global_Runoff_Reconstruction/9228176
- 749 • ESA-CCI Soil Moisture: European Space Agency and Technische Universität Wien
750 (TUW), <https://www.esa-soilmoisture-cci.org/data>
- 751 • MODIS Evapotranspiration: GSFC, NASA,
752 <https://modis.gsfc.nasa.gov/data/dataproduct/mod16.php>
- 753 • GRACE and GRACE-FO: Center for Space Research (CSR), The University of
754 Texas, <https://podaac.jpl.nasa.gov/GRACE>

- 756 Asoka, A., & Mishra, V. (2020). Anthropogenic and Climate Contributions on the
757 Changes in Terrestrial Water Storage in India. *Journal of Geophysical Research:*
758 *Atmospheres*, 125(10). <https://doi.org/10.1029/2020JD032470>
- 759 Attada, R., Kumar, P., & Dasari, H. P. (2018). Assessment of Land Surface Models in a
760 High-Resolution Atmospheric Model during Indian Summer Monsoon. *Pure and*
761 *Applied Geophysics*, 175(10), 3671–3696. <https://doi.org/10.1007/S00024-018->
762 1868-Z/FIGURES/15
- 763 Bates, P. D., Horritt, M. S., & Fewtrell, T. J. (2010). A simple inertial formulation of the
764 shallow water equations for efficient two-dimensional flood inundation modelling.
765 *Journal of Hydrology*, 387(1–2), 33–45.
766 <https://doi.org/10.1016/J.JHYDROL.2010.03.027>
- 767 Bharti, V., & Singh, C. (2015). Evaluation of error in TRMM 3B42V7 precipitation
768 estimates over the himalayan region. *Journal of Geophysical Research*, 120(24),
769 12,458-12,473. <https://doi.org/10.1002/2015JD023779>
- 770 Bhattacharyya, S., Sreekesh, S., & King, A. (2022). Characteristics of extreme rainfall in
771 different gridded datasets over India during 1983–2015. *Atmospheric Research*,
772 267, 105930. <https://doi.org/10.1016/J.ATMOSRES.2021.105930>
- 773 Carrera, M. L., Bélair, S., & Bilodeau, B. (2015). The Canadian Land Data Assimilation
774 System (CaLDAS): Description and synthetic evaluation study. *Journal of*
775 *Hydrometeorology*, 16(3), 1293–1314. <https://doi.org/10.1175/JHM-D-14-0089.1>
- 776 Chakravorty, A., Chahar, B. R., Sharma, O. P., & Dhanya, C. T. (2016). A regional scale
777 performance evaluation of SMOS and ESA-CCI soil moisture products over India
778 with simulated soil moisture from MERRA-Land. *Remote Sensing of Environment*,
779 186, 514–527. <https://doi.org/10.1016/j.rse.2016.09.011>
- 780 Chaudhary, S., Dhanya, C. T., & Vinnarasi, R. (2017). Dry and wet spell variability
781 during monsoon in gauge-based gridded daily precipitation datasets over India.
782 *Journal of Hydrology*, 546, 204–218. <https://doi.org/10.1016/j.jhydrol.2017.01.023>
- 783 De Almeida, G. A. M., Bates, P., Freer, J. E., & Souvignet, M. (2012). *Improving the*
784 *stability of a simple formulation of the shallow water equations for 2-D flood*
785 *modeling*. <https://doi.org/10.1029/2011WR011570>

786 de Goncalves, L. G. G., Shuttleworth, W. J., Burke, E. J., Houser, P., Toll, D. L., Rodell,
787 M., & Arsenault, K. (2006). Toward a South America Land Data Assimilation
788 System: Aspects of land surface model spin-up using the Simplified Simple
789 Biosphere. *Journal of Geophysical Research Atmospheres*, *111*(17).
790 <https://doi.org/10.1029/2005JD006297>

791 Dorigo, W., Wagner, W., Albergel, C., Albrecht, F., Balsamo, G., Brocca, L., Chung,
792 D., Ertl, M., Forkel, M., Gruber, A., Haas, E., Hamer, P. D., Hirschi, M., Ikonen, J.,
793 de Jeu, R., Kidd, R., Lahoz, W., Liu, Y. Y., Miralles, D., ... Lecomte, P. (2017).
794 ESA CCI Soil Moisture for improved Earth system understanding: State-of-the art
795 and future directions. *Remote Sensing of Environment*, *203*, 185–215.
796 <https://doi.org/10.1016/j.rse.2017.07.001>

797 Ek, M. B., Mitchell, K. E., Lin, Y., Rogers, E., Grunmann, P., Koren, V., Gayno, G., &
798 Tarpley, J. D. (2003). Implementation of Noah land surface model advances in the
799 National Centers for Environmental Prediction operational mesoscale Eta model.
800 *Journal of Geophysical Research: Atmospheres*, *108*(D22).
801 <https://doi.org/10.1029/2002JD003296>

802 Funk, C., Peterson, P., Landsfeld, M., Pedreros, D., Verdin, J., Shukla, S., Husak, G.,
803 Rowland, J., Harrison, L., Hoell, A., & Michaelsen, J. (2015). The climate hazards
804 infrared precipitation with stations—a new environmental record for monitoring
805 extremes. *Scientific Data*, *2*(1), 150066. <https://doi.org/10.1038/sdata.2015.66>

806 Gelaro, R., McCarty, W., Suárez, M. J., Todling, R., Molod, A., Takacs, L., Randles, C.
807 A., Darmenov, A., Bosilovich, M. G., Reichle, R., Wargan, K., Coy, L., Cullather,
808 R., Draper, C., Akella, S., Buchard, V., Conaty, A., da Silva, A. M., Gu, W., ...
809 Zhao, B. (2017). The Modern-Era Retrospective Analysis for Research and
810 Applications, Version 2 (MERRA-2). *Journal of Climate*, *30*(14), 5419–5454.
811 <https://doi.org/10.1175/JCLI-D-16-0758.1>

812 Getirana, A. C. V., Boone, A., Yamazaki, D., Decharme, B., Papa, F., & Mognard, N.
813 (2012). The hydrological modeling and analysis platform (HyMAP): Evaluation in
814 the Amazon basin. *Journal of Hydrometeorology*, *13*(6), 1641–1665.
815 <https://doi.org/10.1175/JHM-D-12-021.1>

816 Getirana, A., Jung, H. C., Arsenault, K., Shukla, S., Kumar, S., Peters-Lidard, C.,
817 Maigari, I., & Mamane, B. (2020). Satellite Gravimetry Improves Seasonal

818 Streamflow Forecast Initialization in Africa. *Water Resources Research*, 56(2),
819 e2019WR026259. <https://doi.org/10.1029/2019WR026259>

820 Getirana, A., Kumar, S., Girotto, M., & Rodell, M. (2017). Rivers and Floodplains as
821 Key Components of Global Terrestrial Water Storage Variability. *Geophysical
822 Research Letters*, 44(20), 10,359-10,368. <https://doi.org/10.1002/2017GL074684>

823 Getirana, A., Peters-Lidard, C., Rodell, M., & Bates, P. D. (2017). Trade-off between
824 cost and accuracy in large-scale surface water dynamic modeling. *Water Resources
825 Research*, 53(6), 4942–4955. <https://doi.org/10.1002/2017WR020519>

826 Ghatak, D., Zaitchik, B., Hain, C., & Anderson, M. (2017). The role of local heating in
827 the 2015 Indian Heat Wave. *Scientific Reports*, 7(1), 7707.
828 <https://doi.org/10.1038/s41598-017-07956-5>

829 Ghatak, D., Zaitchik, B., Kumar, S., Matin, M. A., Bajracharya, B., Hain, C., &
830 Anderson, M. (2018a). Influence of Precipitation Forcing Uncertainty on
831 Hydrological Simulations with the NASA South Asia Land Data Assimilation
832 System. *Hydrology*, 5(4), 57. <https://doi.org/10.3390/hydrology5040057>

833 Ghatak, D., Zaitchik, B., Kumar, S., Matin, M. A., Bajracharya, B., Hain, C., &
834 Anderson, M. (2018b). Influence of Precipitation Forcing Uncertainty on
835 Hydrological Simulations with the NASA South Asia Land Data Assimilation
836 System. *Hydrology*, 5(4), 57. <https://doi.org/10.3390/hydrology5040057>

837 Ghiggi, G., Humphrey, V., Seneviratne, S. I., & Gudmundsson, L. (2019). GRUN: An
838 observation-based global gridded runoff dataset from 1902 to 2014. *Earth System
839 Science Data*, 11(4), 1655–1674. <https://doi.org/10.5194/essd-11-1655-2019>

840 Ghodichore, N., Dhanya, C. T., & Hendricks Franssen, H. J. (2022). Isolating the effects
841 of land use land cover change and inter-decadal climate variations on the water and
842 energy cycles over India, 1981–2010. *Journal of Hydrology*, 612, 128267.
843 <https://doi.org/10.1016/J.JHYDROL.2022.128267>

844 Gruber, A., Dorigo, W. A., Crow, W., & Wagner, W. (2017). Triple Collocation-Based
845 Merging of Satellite Soil Moisture Retrievals. *IEEE Transactions on Geoscience
846 and Remote Sensing*, 55(12), 6780–6792.
847 <https://doi.org/10.1109/TGRS.2017.2734070>

848 Gruber, A., Scanlon, T., van der Schalie, R., Wagner, W., & Dorigo, W. (2019).
849 Evolution of the ESA CCI Soil Moisture climate data records and their underlying

850 merging methodology. *Earth System Science Data*, 11(2), 717–739.
851 <https://doi.org/10.5194/essd-11-717-2019>

852 Gupta, P., Verma, S., Bhatla, R., Chandel, A. S., Singh, J., & Payra, S. (2020).
853 Validation of Surface Temperature Derived From MERRA-2 Reanalysis Against
854 IMD Gridded Data Set Over India. *Earth and Space Science*, 7(1),
855 e2019EA000910. <https://doi.org/10.1029/2019EA000910>

856 Hersbach, H., Bell, B., Berrisford, P., Hirahara, S., Horányi, A., Muñoz-Sabater, J.,
857 Nicolas, J., Peubey, C., Radu, R., Schepers, D., Simmons, A., Soci, C., Abdalla, S.,
858 Abellan, X., Balsamo, G., Bechtold, P., Biavati, G., Bidlot, J., Bonavita, M., ...
859 Thépaut, J. (2020). The ERA5 global reanalysis. *Quarterly Journal of the Royal
860 Meteorological Society*, 146(730), 1999–2049. <https://doi.org/10.1002/qj.3803>

861 Hu, Z., Liu, S., Zhong, G., Lin, H., & Zhou, Z. (2020). Modified Mann-Kendall trend
862 test for hydrological time series under the scaling hypothesis and its application.
863 *Hydrological Sciences Journal*, 65(14), 2419–2438.
864 <https://doi.org/10.1080/02626667.2020.1810253>

865 J. L. Monteith. (1965). *Evaporation and environment*.

866 Jacobs, C. M. J., Moors, E. J., ter Maat, H. W., Teuling, A. J., Balsamo, G., Bergaoui,
867 K., Ettema, J., Lange, M., van den Hurk, B. J. J. M., Viterbo, P., & Wergen, W.
868 (2008). Evaluation of European Land Data Assimilation System (ELDAS) products
869 using in situ observations. *Tellus A: Dynamic Meteorology and Oceanography*,
870 60(5), 1023–1037. <https://doi.org/10.1111/j.1600-0870.2008.00351.x>

871 Jin, X., Kumar, L., Li, Z., Feng, H., Xu, X., Yang, G., & Wang, J. (2018). A review of
872 data assimilation of remote sensing and crop models. *European Journal of
873 Agronomy*, 92, 141–152. <https://doi.org/10.1016/j.eja.2017.11.002>

874 Kantha Rao, B., & Rakesh, V. (2019). Evaluation of WRF-simulated multilevel soil
875 moisture, 2-m air temperature, and 2-m relative humidity against in situ
876 observations in India. *Pure and Applied Geophysics*, 176(4), 1807–1826.
877 <https://doi.org/10.1007/s00024-018-2022-7>

878 Kim, N. H., & Office, N. D. (2017). *Global Soil Wetness Project Phase 3 Atmospheric
879 Boundary Conditions (Experiment 1)*. <https://doi.org/10.20783/DIAS.501>

880 Kirchner, J. W. (2006). Getting the right answers for the right reasons: Linking
881 measurements, analyses, and models to advance the science of hydrology. *Water*
882 *Resources Research*, 42(3). <https://doi.org/10.1029/2005WR004362>

883 Knoben, W. J. M., Freer, J. E., & Woods, R. A. (2019). Technical note: Inherent
884 benchmark or not? Comparing Nash–Sutcliffe and Kling–Gupta efficiency scores.
885 *Hydrology and Earth System Sciences*, 23(10), 4323–4331.
886 <https://doi.org/10.5194/hess-23-4323-2019>

887 Kumar, S., Peterslidard, C., Tian, Y., Houser, P., Geiger, J., Olden, S., Lighty, L.,
888 Eastman, J., Doty, B., & Dirmeyer, P. (2006). Land information system: An
889 interoperable framework for high resolution land surface modeling. *Environmental*
890 *Modelling & Software*, 21(10), 1402–1415.
891 <https://doi.org/10.1016/j.envsoft.2005.07.004>

892 Kumar, S. v, Peters-Lidard, C. D., Mocko, D., Reichle, R., Liu, Y., Arsenault, K. R.,
893 Xia, Y., Ek, M., Riggs, G., Livneh, B., & Cosh, M. (2014). Assimilation of
894 Remotely Sensed Soil Moisture and Snow Depth Retrievals for Drought
895 Estimation. *Journal of Hydrometeorology*, 15(6), 2446–2469.
896 <https://doi.org/10.1175/JHM-D-13-0132.1>

897 Landerer, F. W., & Swenson, S. C. (2012). Accuracy of scaled GRACE terrestrial water
898 storage estimates. *Water Resources Research*, 48(4).
899 <https://doi.org/10.1029/2011WR011453>

900 Lohmann, D., Mitchell, K. E., Houser, P. R., Wood, E. F., Schaake, J. C., Robock, A.,
901 Cosgrove, B. A., Sheffield, J., Duan, Q., Luo, L., Higgins, R. W., Pinker, R. T., &
902 Tarpley, J. D. (2004). Streamflow and water balance intercomparisons of four land
903 surface models in the North American Land Data Assimilation System project.
904 *Journal of Geophysical Research: Atmospheres*, 109(D7).
905 <https://doi.org/10.1029/2003JD003517>

906 Maina, F. Z., Kumar, S. V., Albergel, C., & Mahanama, S. P. (2022). Warming, increase
907 in precipitation, and irrigation enhance greening in High Mountain Asia.
908 *Communications Earth & Environment*, 3(1), 43. [https://doi.org/10.1038/s43247-](https://doi.org/10.1038/s43247-022-00374-0)
909 [022-00374-0](https://doi.org/10.1038/s43247-022-00374-0)

910 Maity, S., Satyanarayana, A. N. V., Mandal, M., & Nayak, S. (2017). Performance
911 evaluation of land surface models and cumulus convection schemes in the
912 simulation of Indian summer monsoon using a regional climate model.

913 *Atmospheric Research*, 197, 21–41.
914 <https://doi.org/10.1016/J.ATMOSRES.2017.06.023>

915 Mann, H. B. (1945). Nonparametric Tests Against Trend. *Econometrica*, 13(3), 245.
916 <https://doi.org/10.2307/1907187>

917 Mccollum, J. R., & Ferraro, R. R. (2005). *Microwave Rainfall Estimation over Coasts*.
918 <https://doi.org/10.1175/JTECH1732.1>

919 McNally, A., Arsenault, K., Kumar, S., Shukla, S., Peterson, P., Wang, S., Funk, C.,
920 Peters-Lidard, C. D., & Verdin, J. P. (2017). A land data assimilation system for
921 sub-Saharan Africa food and water security applications. *Scientific Data*, 4(1),
922 170012. <https://doi.org/10.1038/sdata.2017.12>

923 Mizukami, N., Rakovec, O., Newman, A. J., Clark, M. P., Wood, A. W., Gupta, H. v, &
924 Kumar, R. (2019). On the choice of calibration metrics for “high-flow” estimation
925 using hydrologic models. *Hydrology and Earth System Sciences*, 23(6), 2601–2614.
926 <https://doi.org/10.5194/hess-23-2601-2019>

927 Nair, A. S., & Indu, J. (2019). Improvement of land surface model simulations over
928 India via data assimilation of satellite-based soil moisture products. *Journal of*
929 *Hydrology*, 573, 406–421. <https://doi.org/10.1016/J.JHYDROL.2019.03.088>

930 Newman, A. J., Stone, A. G., Saharia, M., Holman, K. D., Addor, N., & Clark, M. P.
931 (2021). Identifying sensitivities in flood frequency analyses using a stochastic
932 hydrologic modeling system. *Hydrology and Earth System Sciences*, 25(10), 5603–
933 5621. <https://doi.org/10.5194/hess-25-5603-2021>

934 Niu, G. Y., Yang, Z. L., Mitchell, K. E., Chen, F., Ek, M. B., Barlage, M., Kumar, A.,
935 Manning, K., Niyogi, D., Rosero, E., Tewari, M., & Xia, Y. (2011). The
936 community Noah land surface model with multiparameterization options (Noah-
937 MP): 1. Model description and evaluation with local-scale measurements. *Journal*
938 *of Geophysical Research Atmospheres*, 116(12).
939 <https://doi.org/10.1029/2010JD015139>

940 Niu, G.-Y., Yang, Z.-L., Dickinson, R. E., Gulden, L. E., & Su, H. (2007). Development
941 of a simple groundwater model for use in climate models and evaluation with
942 Gravity Recovery and Climate Experiment data. *Journal of Geophysical Research:*
943 *Atmospheres*, 112(D7). <https://doi.org/10.1029/2006JD007522>

944 Pai, D. S., Sridhar, L., Rajeevan, M., Sreejith, O. P., Satbhai, N. S., & Mukhopadhyay,
945 B. (2014). *Development of a new high spatial resolution (0.25° × 0.25°) long*
946 *period (1901-2010) daily gridded rainfall data set over India and its comparison*
947 *with existing data sets over the region* (Vol. 65, Issue 1).

948 Patil, M. N., Waghmare, R. T., Halder, S., & Dharmaraj, T. (2011). Performance of
949 Noah land surface model over the tropical semi-arid conditions in western India.
950 *Atmospheric Research*, 99(1), 85–96.
951 <https://doi.org/10.1016/J.ATMOSRES.2010.09.006>

952 Rodell, M., Houser, P. R., Berg, A. A., & Famiglietti, J. S. (2005). Evaluation of 10
953 Methods for Initializing a Land Surface Model. *Journal of Hydrometeorology*, 6(2),
954 146–155. <https://doi.org/10.1175/JHM414.1>

955 Rodell, M., Houser, P. R., Jambor, U., Gottschalck, J., Mitchell, K., Meng, C.-J.,
956 Arsenault, K., Cosgrove, B., Radakovich, J., Bosilovich, M., Entin, J. K., Walker, J.
957 P., Lohmann, D., & Toll, D. (2004). The Global Land Data Assimilation System.
958 *Bulletin of the American Meteorological Society*, 85(3), 381–394.
959 <https://doi.org/10.1175/BAMS-85-3-381>

960 Roy, P., Martha, T. R., Vinod Kumar, K., Chauhan, P., & Rao, V. V. (2023). Cluster
961 landslides and associated damage in the Dima Hasao district of Assam, India due to
962 heavy rainfall in May 2022. *Landslides*, 20(1), 97–109.
963 <https://doi.org/10.1007/S10346-022-01977-6/METRICS>

964 Running, S. W., Mu, Q., Zhao, M., & Moreno, A. (2019). *User's Guide MODIS Global*
965 *Terrestrial Evapotranspiration (ET) Product (MOD16A2/A3 and Year-end Gap-*
966 *filled MOD16A2GF/A3GF) NASA Earth Observing System MODIS Land*
967 *Algorithm (For Collection 6)*.

968 Saharia, M., Jain, A., Baishya, R. R., Haobam, S., Sreejith, O. P., Pai, D. S., &
969 Rafieeinasab, A. (2021). India flood inventory: creation of a multi-source national
970 geospatial database to facilitate comprehensive flood research. *Natural Hazards*,
971 108(1), 619–633. <https://doi.org/10.1007/s11069-021-04698-6>

972 Satish Kumar, K., AnandRaj, P., Sreelatha, K., & Sridhar, V. (2023). Reconstruction of
973 GRACE terrestrial water storage anomalies using Multi-Layer Perceptrons for
974 South Indian River basins. *Science of The Total Environment*, 857, 159289.
975 <https://doi.org/10.1016/J.SCITOTENV.2022.159289>

- 976 Sawada, Y., & Koike, T. (2016). Ecosystem resilience to the Millennium drought in
977 southeast Australia (2001–2009). *Journal of Geophysical Research:*
978 *Biogeosciences*, 121(9), 2312–2327. <https://doi.org/10.1002/2016JG003356>
- 979 Shah, H. L., & Mishra, V. (2016). *Uncertainty and Bias in Satellite-Based Precipitation*
980 *Estimates over Indian Subcontinental Basins: Implications for Real-Time*
981 *Streamflow Simulation and Flood Prediction**. <https://doi.org/10.1175/JHM-D-15>
- 982 Shepard, D. (1968). A two-dimensional interpolation function for irregularly-spaced
983 data. 1968, 517–524.
- 984 Soni, A., & Syed, T. H. (2015). Diagnosing Land Water Storage Variations in Major
985 Indian River Basins using GRACE observations. *Global and Planetary Change*,
986 133, 263–271. <https://doi.org/10.1016/j.gloplacha.2015.09.007>
- 987 Srivastava, A., Sahoo, B., Raghuwanshi, N. S., & Singh, R. (2017). Evaluation of
988 Variable-Infiltration Capacity Model and MODIS-Terra Satellite-Derived Grid-
989 Scale Evapotranspiration Estimates in a River Basin with Tropical Monsoon-Type
990 Climatology. *Journal of Irrigation and Drainage Engineering*, 143(8).
991 [https://doi.org/10.1061/\(asce\)ir.1943-4774.0001199](https://doi.org/10.1061/(asce)ir.1943-4774.0001199)
- 992 Tellus. (2018). *TELLUS_GRACE_MASCON_CRI_GRID_RL06_VI*.
- 993 Upadhyaya, D. B., Evans, J., Muddu, S., Tomer, S. K., Bitar, A. Al, Yeggina, S., S, T.,
994 Morrison, R., Fry, M., Tripathi, S. N., Mujumdar, M., Goswami, M., Ganeshi, N.,
995 Nema, M. K., Jain, S. K., Angadi, S. S., & Yenagi, B. S. (2021). The Indian
996 COSMOS Network (ICON): Validating L-Band Remote Sensing and Modelled
997 Soil Moisture Data Products. *Remote Sensing 2021, Vol. 13, Page 537*, 13(3), 537.
998 <https://doi.org/10.3390/RS13030537>
- 999 Watkins, M. M., Wiese, D. N., Yuan, D. N., Boening, C., & Landerer, F. W. (2015).
1000 Improved methods for observing Earth's time variable mass distribution with
1001 GRACE using spherical cap mascons. *Journal of Geophysical Research: Solid*
1002 *Earth*, 120(4), 2648–2671. <https://doi.org/10.1002/2014JB011547>
- 1003 Xia, Y., Hao, Z., Shi, C., Li, Y., Meng, J., Xu, T., Wu, X., & Zhang, B. (2019). Regional
1004 and Global Land Data Assimilation Systems: Innovations, Challenges, and
1005 Prospects. *Journal of Meteorological Research*, 33(2), 159–189.
1006 <https://doi.org/10.1007/s13351-019-8172-4>

1007 Yamazaki, D., Ikeshima, D., Tawatari, R., Yamaguchi, T., O’Loughlin, F., Neal, J. C.,
1008 Sampson, C. C., Kanae, S., & Bates, P. D. (2017). A high-accuracy map of global
1009 terrain elevations. *Geophysical Research Letters*, 44(11), 5844–5853.
1010 <https://doi.org/10.1002/2017GL072874>

1011 Yoon, Y., Kumar, S. V., Forman, B. A., Zaitchik, B. F., Kwon, Y., Qian, Y., Rupper, S.,
1012 Maggioni, V., Houser, P., Kirschbaum, D., Richey, A., Arendt, A., Mocko, D.,
1013 Jacob, J., Bhanja, S., & Mukherjee, A. (2019). Evaluating the Uncertainty of
1014 Terrestrial Water Budget Components Over High Mountain Asia. *Frontiers in*
1015 *Earth Science*, 7. <https://doi.org/10.3389/feart.2019.00120>

1016 Yucel, I., Onen, A., Yilmaz, K. K., & Gochis, D. J. (2015). Calibration and evaluation of
1017 a flood forecasting system: Utility of numerical weather prediction model, data
1018 assimilation and satellite-based rainfall. *Journal of Hydrology*, 523, 49–66.
1019 <https://doi.org/10.1016/j.jhydrol.2015.01.042>

1020 Zhang, X., Obringer, R., Wei, C., Chen, N., & Niyogi, D. (2017). Droughts in India
1021 from 1981 to 2013 and Implications to Wheat Production. *Scientific Reports*, 7(1),
1022 44552. <https://doi.org/10.1038/srep44552>

1023 Zhao, W., & Li, A. (2015). A Review on Land Surface Processes Modelling over
1024 Complex Terrain. *Advances in Meteorology*, 2015, 1–17.
1025 <https://doi.org/10.1155/2015/607181>

1026